NTNU

Norwegian University of
Science and Technology

A Numerical and Analytical Investigation of the Relation Between Transport Properties and Grain Size Distribution

Kristian Engeskaug

Petroleum Geoscience and Engineering
Submission date: June 2018
Supervisor: Carl Fredrik Berg, IGP

Norwegian University of Science and Technology
Department of Geoscience and Petroleum

Summary

There have been many and varied attempts describing the relation between transport and rock properties for porous materials, including the work of Kozeny (1927), Carman (1938), and Berg (1970). Common features of these efforts are that the developed equations all contain adjustable parameters that need to be determined for a given data set. Despite that these equations are approximations, they are widely used for engineering calculations due to the importance of linking transport and rock properties.

Pore scale modeling and simulation offers the possibility to investigate the relation between grain size distribution and transport properties in a controlled environment. Two different strategies for expressing permeability were used in this study. The first approach was to express permeability using statistical characteristics of the grain size distribution. We used the e-Core software to generate a set of sphere packs with grain size distributions described by a volume-weighted mean and standard deviation. The obtained transport description yields reasonable results for sphere packs, while it has limited applicability to natural porous media.

The second approach relies on describing the inscribed diameter between three grains of a pore throat. Three points from a grain size distribution was randomly chosen, and the inscribed diameter determined. From this, a cumulative pore throat area distribution was developed. Assuming that the number of pore throats along a streamline between the inlet and outlet of the porous medium can be approximated as the length of the medium divided by the average grain size, we found an effective pore throat size as the harmonic mean of a set of random inscribed diameters. The variance of these diameters and the expected inscribed pore diameter was employed to estimate the permeability.

Both approaches have been compared to earlier attempts correlating transport and pore structure. Although all the methods are approximations, they give valuable insight into the relation between pore structure and transport.

Sammendrag

Gjennom historien har det vært flere forsøk på å beskrive relasjonen mellom transport- og bergartsegenskaper for porøse medier. Dette inkluderer arbeidene utført av Kozeny (1927), Carman (1938) og Berg (1970). Fellesnevneren for disse arbeidene har vært at hver ligning har inneholdt en parameter som må justeres i henhold til dataene. Selv om disse ligningene er tilnærminger, brukes de i vid utstrekning i ingeniørberegninger. Dette indikerer viktigheten av å koble bergarts- og transportegenskaper sammen.

Simulering og modulering på poreskalanivå gir muligheten til å utforske relasjonen mellom kornstørrelsesfordelinger og transportegenskaper i et kontrollert miljø. I denne studien er det benyttet to ulike fremgangsmåter. Den første innebærer å beskrive permeabilitet ved å bruke statistiske karakteristikker fra en kornstørrelsesfordeling. Vi brukte programvaren, e-Core, for å generere et sett med sfærepakker. Disse ble generert med en kornstørrelsesfordeling som var volumvektet basert på datasettets gjennomsnittlige kornstørrelse og standardavvik. Den utviklede ligningen gir gode resultater for sfærepakkene, men har begrenset anvendbarhet på ekte porøse medier.

Den andre fremgangsmåten beskriver den inskriberte diameter mellom tre korn i en porehals. Tre tilfeldige punkter fra en kornstørrelsesfordeling ble valgt og den inskriberte diameteren beregnet. Dette gir en kumulativ porehalsdistribusjon. Om vi antar at antall porehalser langs en strømlinje mellom inn- og utløp for det porøse mediet kan bli tilnærmet som lengden til modellen delt på gjennomsnittlig kornstørrelse, finner vi en effektiv porehals. Denne er beskrevet som det harmoniske gjennomsnittet av et sett av tilfeldige inskriberte porediametre. Variansen til disse diametrene og den forventede verdien av inskribert porediameter ble anvendt for å estimere permeabilitet.

Begge fremgangsmåtene har blitt sammenlignet med tidligere forsøk på å korrelere porestruktur med transportegenskaper. På tross av at alle disse metodene er tilnærminger, gir de verdifull innsikt i relasjonen mellom transportegenskaper og porestruktur.

Acknowledgement

This master thesis is written at the Department of Geoscience and Petroleum (IGP), Norwegian University of Science and Technology (NTNU). It is the final product of the master program in Geoscience and Engineering, with specialization in Reservoir Engineering and Petrophysics.

There are several people that have been involved in this thesis and I would like to express my gratitude to those who have contributed. Firstly, I would like to thank my supervisor, Associate Professor Carl Fredrik Berg, for providing me an interesting and intriguing topic for this master thesis. Thanks for sharing your knowledge, advice and for frequently following up my work. It is highly appreciated. Secondly, thanks to fellow students at the office for assistance, interesting discussions and fun stories.

Kristian Engeskaug
Trondheim, June 2018

TABLE OF CONTENTS

LIST OF TABLES

LIST OF FIGURES

Nomenclature

Abbreviations

CDF	=	Cumulative distribution function
CPU	=	Central processing unit
CT	=	Computed tomography
DRP	=	Digital rock physics
erf	=	Error function
GSD	=	Grain size distribution
MGS	=	Mean grain size
PD	=	Percentile deviation
SD	=	Standard deviation
SEM	=	Scanning electron microscope
VW	=	Volume weighted

Symbols

∇	=	Gradient

Greek Letters

α	=	Angle
β	=	Angle
γ	=	Angle
γ	=	Surface tension
Δ	=	Differential
θ	=	Contact angle
κ	=	Temperature and liquid function
μ	=	Viscosity
μ	=	Mean
ρ	=	Density
σ	=	Standard deviation
σ	=	Conductance
τ	=	Tortuosity
Φ	=	Phi distribution function
ϕ	=	Porosity

Roman Letters

A	=	Area
a	=	Constant
b	=	Bottom line
c	=	Constant
c	=	Value
C	=	Constriction factor
d	=	Diameter
d	=	Constant
E	=	Expected
e	=	Exponential function
F	=	Formation factor
G	=	Shape factor
g	=	Conductivity
g	=	Gravitational acceleration
h	=	Height
h	=	Head
k	=	Permeability
l	=	Length
Md	=	Median
m	=	Cementation exponent
N	=	Number
n	=	Number
p	=	Pressure
R	=	Constant
R	=	Resistivity
r	=	Radius
S	=	Streamline
S	=	Surface area
S	=	Circle sector
s	=	Circumference
Δs	=	Length of porous medium
u	=	Interstitial velocity
Q	=	Flow rate
$\overline{x}$	=	Average
x	=	Observed grain size value

Subscripts

10	=	10% weighting
a	=	air
abs	=	Absolute
c	=	Characteristic
exp	=	Expected
h	=	Hydraulic
i	=	Step indicator
insc	=	Inscribed
mean	=	Mean value
o	=	Rock resistivity
S	=	Streamline
Sys	=	System
t	=	Threshold
w	=	Brine
w	=	Water

CHAPTER 1

INTRODUCTION

A proper understanding of the transport properties of fluid in porous media is of great importance in science and technology. Transport properties in porous media are not only a central part in establishing producibility of petroleum reservoirs. Flow in porous media also governs fuel cells, thermoelectric cells, gels and even the human body (Katz and Thompson, 1986; PoreLab, 2018). Therefore, one can say that description of flow in porous media is important for geological, technological and biological purposes. This thesis aims to give a better description of transport properties from a geological point of view.

It is the microscopic features of porous media that determine several of the macroscopic properties such as permeability and formation factor (Øren et al., 1998). Based on this it should be possible to describe the macroscopic properties using a precise description of the physical processes on a pore scale level. Throughout history there have been many attempts to derive a general relationship relating permeability to reservoir rock properties. The existing equations are empirical descriptors of flow in porous media and no proven theoretical relationship is developed (Fatt, 1956; Scheidegger, 1957). Equations have in general been developed based on quite elementary geometrical models from the pore space. The two most common models has been the bundle of tubes and the sphere pack model.

Poiseuille and Darcy were two of the pioneers doing research of flow in porous media. They did not relate their equations directly to rocks, but relied on theoretical models. In 1846, Poiseuille described fluid flow through small pipes (as restated in Sutera and Skalak (1993)), while Darcy (1856) described flow through capillary tubes filled with sand. Later,

in 1892 Hazen derived an expression relating flow to a constant multiplied with grain radius squared (Hazen, 1895). This was later supported by Slichter (1899) who concluded that permeability should be proportional to the square of grain diameter and to a factor that was based on the packing of the grains.

In more modern times, Krumbein and Monk (1943) studied the size parameters and derived an equation for permeability. Beard and Weyl (1973) studied the effect of texture on porosity and permeability and concluded that both vary with sorting, and that low sphericity and high angularity increases them. Berg (1970) derived an equation valid for clean quartz rich sandstones as a function of porosity and mean grain diameter, resembling Slichters equation from 1899. Hence, the structure of the equations has not changed much the last 100 years. In *The physics of flow through porous media*, Scheidegger (1957) concludes that no generic relationship between porosity and permeability has yet been revised. The empirical equations existing fail to give satisfactory results due to their narrow applicability. A generic relationship is believed to have a great theoretical and practical application.

The work to be reported in this thesis is undertaken with the belief that studying a pore scale model that more realistically describes porous media will give a better understanding of flow and on the factors that affect it. We propose an approach of randomly distributed inscribed pore-diameters mimicking flow channels of porous media. From these diameters we find the variance and an expression for the expected inscribed pore diameter. To evaluate the transport properties requires use of appropriate software. The final result is an equation describing the permeability using expected inscribed pore diameter and the variance of a set of mean inscribed diameters.

1.1 Thesis Overview

This master thesis is a continuation of the specialization project from the fall of 2017 (Engeskaug, 2017). Therefore, some of the material presented is revised from the specialization project.

In chapter 2 and 3 the needed theory is presented. Chapter 2 focuses on basic theory and gives an overview of terms and basic properties, while chapter 3 is more specified directly to the work in this thesis. Section 2.1-2.3 along with section 2.8-2.10 and 2.12.1 in the background is revised from the project thesis. The methodology and approach is described in chapter 4, where section 4.1 is methodology revised from the project thesis. Results of the work is presented in chapter 5 and discussed in 6. At last the conclusion of

the study is presented in chapter 7 and recommendations for further work can be found in chapter 8.

CHAPTER 2
BACKGROUND

In this section theory and background for the objective and ambition of this thesis is presented. It includes basic concepts of pore scale measurements and parameters as well as preceding methods for estimating transport properties in porous media.

2.1 Reservoir Rock Properties

Most reservoir rocks are sedimentary in origin, meaning, they were deposited as sediments accumulated over time. Sedimentary rocks that contain oil and gas are most usually clastic, chemical or organic sedimentary rocks (King, 2017). Chemical and organic sedimentary rocks include limestone and dolomite among others, formed from dissolution, precipitation or accumulation of organic materials, while clastic rocks are clasts or fragments of existing minerals and rock. Sandstones are a clastic sedimentary rock, and is today the most common petroleum reservoir. A sandstone is defined to constitute of more than 50% of sand-sized ($\leq$1-2mm) rock grains and minerals (Hu et al., 2017). It is well established that reservoir rocks, such as sandstones, are characterized by a broad distribution of grain sizes, and thus pore sizes. All clastic rocks have three main properties; composition, sedimentary structure and texture. In his paper, Berg (1970) declares composition as fundamental and that it decides the texture, while the sedimentary structures controls the homogeneity of the distribution of the elements of texture and composition. The elements of texture are sorting, grain size, shape, packing and orientation (Berg, 1970). More easily, one can say that the texture describes the framework, structure and arrangement of the rock.

Texture and composition has a vital influence on the main reservoir properties; porosity and permeability. Knowing the texture of a reservoir rock is key as it can help interpret mechanisms and environments at deposition. The physical properties of reservoir rocks are relying on the framework of the grains, particularly on grain composition and texture of the rock. Knowledge of these properties for a reservoir rock is thus of importance for a reservoir engineer. Another important aspect is the ability to connect geology to reservoir properties, to be able to build realistic reservoir models.

2.2 Grain Size Distribution (GSD)

Results of a grain size sieve analysis are commonly displayed graphically, but sometimes presented in a table. Usually it's presented as is displayed in figure 2.1. The illustration is of cumulative distribution curves.

One of the key properties from a grain size distribution is the sorting. It is a measure of the range or dispersion of grain sizes present in the rock. A low standard deviation indicates that the grain sizes are close to the mean grain size (or expected grain size) of the rock. When a GSD is presented as cumulative, the incline of the curve portrays the sorting of the rock: A steeper curve reflects a more uniform grain size, while a gentle slope reflects a less homogeneous grain size.

Sieve Analysis and Statistical Properties

The most traditional and best-known method for determining the particle size distribution is sieve analysis. This method divides the grains into size fractions, and determines the weight of them. Sieve analysis is known to be reliable and quick.

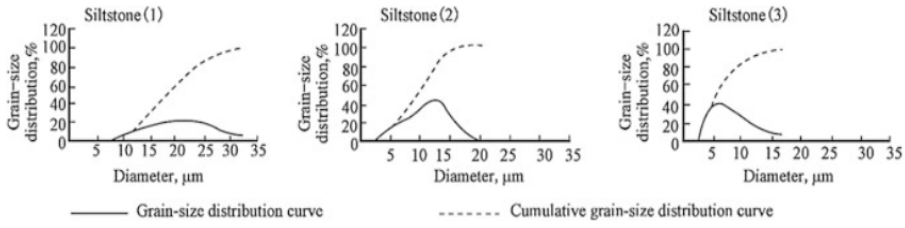

Figure 2.1: Grain size distributions for different siltstones presented through cumulative distribution curves (Hu et al., 2017).

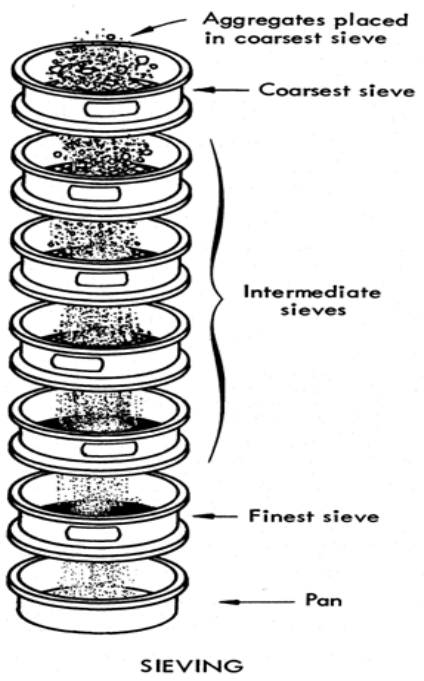

Figure 2.2: Apparatus used in traditional sieve analysis (Jualbatusplit, 2014).

During a sieve analysis, the sample is first crushed, then subjected for shaking (Retsch GmbH & Co. KG , 2004). Depending on their size, the grains will either pass through the sieve or retain on the sieve surface. The final result is a distribution representing the size fractions and their weight. A simple schematic of the apparatus used in a sieve analysis is illustrated in figure 2.2.

The cumulative distribution function (CDF) from the normal distribution is expressed as follows:

$$F(x) = \frac{1}{2}\left[1 + erf\left(\frac{x-\mu}{\sigma\sqrt{2}}\right)\right], \tag{2.1}$$

where x is the observed grain size values, μ is the mean and σ is the standard deviation. The error function (erf) is described as:

$$erf(x) = \frac{2}{\sqrt{\pi}}\int_0^x e^{-t^2}dt, \tag{2.2}$$

And the arithmetic mean and standard deviation is expressed respectively as:

$$\mu = \frac{1}{n}\sum_{i=1}^{n} c_i, \tag{2.3}$$

$$\sigma = \sqrt{\frac{\sum_{i=1}^{N}(x_i - \overline{x})^2}{N-1}}. \tag{2.4}$$

Lastly, the harmonic mean is expressed as:

$$\mu = \frac{n}{\sum_{i=1}^{n} \frac{1}{x_i}}, \tag{2.5}$$

A general understanding of grain size distributions and it's statistical properties will make it easier to interpret results obtained from simulations.

2.3 Mercury Intrusion Porosimetry

There exist different methods for determining the pore sizes of a rock, such as gas adsorption and use of a scanning electron microscope (SEM), while the most common method is mercury intrusion porosimetry. Mercury intrusion porosimetry, in addition to give a measure of porosity, provides a pore size distribution. The apparatus is illustrated in figure 2.3. First, a core is dried to remove any fluid present within the core. The sample is weighed and placed in a chamber, which is then evacuated, and mercury is introduced surrounding the core sample. The pressure is increased step-wise, and the intrusion of mercury is monitored for each step. The monitored volumes of intruded mercury and the pressure steps provide the required data for a pore size distribution (Diamond, 2000).

To obtain a pore size distribution the measured data must be inserted in an appropriate model. For every step of applied pressure, the diameter of the intruded pores is determined by the Young-Laplace equation for cylindrical tubes.

$$d = -\frac{4\gamma cos(\theta)}{p}, \tag{2.6}$$

where d is the diameter of the pore cylinder, γ is the surface tension of mercury, θ is the contact angle of mercury on the solid and p is the applied pressure. By applying this equation, a pore size distribution is obtained from the pressure versus the intrusion data.

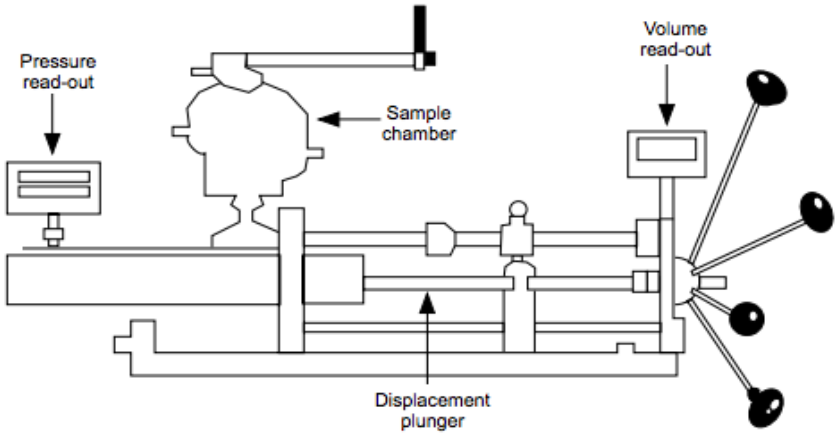

Figure 2.3: Volumetric mercury displacement pump (American Petroleum Institute, 1998).

2.4 Hagen-Poiseuille

Jean Léonard Marie Poiseuille performed a series of experiments on flow in tubes in the early to mid 1800's. He pursued to find a functional relationship between four variables. These were the volumetric flow rate out of a tube, Q, the driving pressure p and the diameter, d and length of the tube, l (Sutera and Skalak, 1993). From his experiments he was able to express the volumetric flux as:

$$Q = \frac{\kappa \Delta p d^4}{l}, \tag{2.7}$$

where κ is a function of temperature and the liquid. In 1839, Gotthilf Heinrich Ludwig Hagen, published his work on flow in cylindrical pipes. His results were closely related to Poiseuilles, but were less accurate, although they included entry effects and distinction between laminar and turbulent flow (Sutera and Skalak, 1993). The results of Hagen and Poiseuille closely agreed and the law of laminar flow was formed, and it was called the Hagen-Poiseuille law. Today, the majority know it as Poiseuilles law and it is similar to equation 2.7, but the constant κ is not included and d is exchanged with r:

$$\Delta p = \frac{8 \mu Q l}{\pi r^4}, \tag{2.8}$$

where Δp is the pressure difference between inlet and outlet, μ is the viscosity, Q is the flow rate, l is the cylinder length and r is the cylinder radius. The equation is valid for laminar flow, and is thus suitable for describing flow in porous media (Xiong et al., 2016).

2.5 Hydraulic Conductance

Hydraulic conductivity of a rock is the property that describes the ease of fluids, such as oil or water, to move through it's pores (Mualem, 1976). The conductivity, g, is dependent on the permeability of the rock, saturation and the density and viscosity of the fluid. Hagen-Poiseuilles law can be used to express conductivity, by describing the relationship between the flow rate, Q, and the driving force, Δp. By assuming that the pore throat can be modeled as a cylindrical tube with a constant cross sectional area, we can rearrange equation 2.8, and substitute $\pi r^4 = \frac{A^2}{\pi}$:

$$g = \frac{\pi r^4}{8\mu l} \overset{\mu=1}{=} \frac{A^2}{8\pi l}, \tag{2.9}$$

where the viscosity is assumed to be μ=1. This is a sound assumption as this is the value of water, but is also within the range of oil viscosities (Beal, 1946).

2.6 Shape Factor

The approach presented in this thesis regards one-phase flow in porous media, but it is evident that reservoirs experience multiphase flow. This may be oil, water and gas or chemical injection fluids. A general feature common for all porous media is the occurrence of angular pores and crevices. The wetting fluid of the pores is retained in the corners allowing flow of other fluids simultaneously through the pore. This effect is due to capillary behavior and regards for multiphase flow. With a one-phase flow the supporting reason to implement a shape factor is the effect of velocity through different geometrical shapes. If we consider two pores with exact same area, but different shape and that the surface velocity is zero, we will have different velocities through each of them depending on average distance from the pore wall. In early research, experiments where cylinders were filled with loose sand were common practice, such as Darcy's (1856) experiment. A more realistic approach is to model the cross section of the pores as non-circular shapes. This incorporates the effect of angularities and crevices (Øren et al., 1998). A complete inclusion of the effect of angular pores and crevices is not possible, but by utilizing the shape factor a more representative model of the porous media is obtained. Mason and Morrow (1991) defined the dimensionless shape factor, G, as:

$$G = \frac{A}{s^2}, \tag{2.10}$$

where A is the cross section area of the pore and s is the pore circumference. From the equation it is obvious that the shape factor value will be reduced as the pores become more

irregular. For triangles, the shape factor ranges from zero for a slit based pore to 0.048 for an equilateral triangle shaped pore. For a circle the shape factor is $\frac{1}{4\pi}$, while it is $\frac{1}{16}$ for rectangles.

Øren et al. (1998) did conductance computations on a multiple of triangular pores. They discovered that there was a functional dependency between the shape factor, G and conductance. The dependence is close to linear and is approximated as:

$$g = \frac{3}{5}\frac{A^2 G}{\mu} = \frac{3}{5}A^2 G, \tag{2.11}$$

where A is the cross sectional area of the pore body.

2.7 Formation Factor and Electrical Conductance

In his article, Archie (1942) studies the electrical resistivity log and how this can be applied to characterize some reservoir properties. An essential part of electrical resistivity log interpretation is the electrical conductivity of brine filled sedimentary rock, as this is vital for petroleum exploration (Berg, 2012). Archie studied the resistivities of a large number of brine-saturated cores from various formations. The cores ranged from 10 to 40 percent porosity and with a salinity of the electrolyte ranging from 20000 to 100000 milligrams NaCl/liter. From his experience, Archie (1942) found the simple relation:

$$F = \frac{R_o}{R_w}, \tag{2.12}$$

where F is the formation resistivity factor, R_o is the electrical resisitivity of the rock saturated with brine and R_w is the resistivity of the brine. From his data Archie (1942) also formulated an empirical relation between the porosity ϕ and formation resistivity factor F to describe the conductivity of a porous medium. It is given as:

$$F = \phi^{-m} \tag{2.13}$$

where m is the cementation exponent. This exponent is found to range from 1.8-2.0 for consolidated sandstones (Archie, 1942).

2.8 Tortuosity, τ

The formation factor described in the previous section measures the influence of pore structure on resistivity. Another property describing the pore structure is the tortuosity. Tortuosity is the measure of the geometric complexity in a porous medium. It characterizes

the tangled pathways of fluid diffusion and electrical conduction through porous media and is a measure of deviation from the shortest possible path (Bellini et al., 2018). When considering fluid dynamics, tortuosity is expressed as the length of the porous medium (Δs) divided by the streamline (S) length (l_S) (Berg, 2014), i.e:

$$\tau(S) = \Delta s / l_S. \tag{2.14}$$

If considering an ideal porous media with one single circular pipe of constant cross-sectional area, where l_s is the length connecting the opposite sides and the length of the cube is Δs. Then, one can express the formation factor, F as (Berg, 2012):

$$F = 1/(\tau^2 \phi), \tag{2.15}$$

where ϕ is the porosity.

2.9 Constriction Factor

The tortuosity as described above accounts for the circuitous path through a rock, while the constriction factor accounts for the decrease in permeability due to variations in local fluid velocities as an effect of the pore constrictions within a rock. Berg (2014) defined the constriction factor as:

$$C(S) = \frac{1}{l_S^2} \int_S \frac{\nabla h \cdot \mathbf{u}}{u} ds \int_S \frac{u}{\nabla h \cdot \mathbf{u}} ds = \frac{1}{l_S^2} \nabla h \int_S \frac{u}{\Delta h \cdot \mathbf{u}} ds, \tag{2.16}$$

where u is the interstitial velocity. Both tortuosity and the constriction factor are only dependent on pore structure and overall direction of flow.

2.10 Size Parameters and Their Effect on Permeability and Porosity

On a pore scale level, the primary properties of a detrital rock are texture, composition and sedimentation. Of these three properties, texture has the largest influence when determining a rocks ability to contain and transmit fluids. The elements of texture are sorting, grain size, shape, orientation and packing (Berg, 1970). There are several factors governing both porosity and permeability. Some factors have a larger impact on the one than the other. The following theory highlights some of the factors regarding porosity and permeability conditions in assemblages of uniform spheres, and comparison with natural deposits. It

is important to remember that such an assemblage of spheres is a simplification of real porous media and will never replicate nature exactly.

Grain size influences the porosity of natural assemblies. As grain size decreases, the ratio of surface area to volume and mass becomes higher, making friction, adhesion and bridging (fines migrate to create ”bridges” between grains) important (Fraser, 1935). Therefore, the smaller the grain size, the greater the porosity. Slichter (1899) was one of the earliest to quantify the effect of grain size on permeability. He concluded that the rate of flow through a column of spheres is directly proportional to the square of the diameter of the spheres and to a factor based on the packing. The diameter squared relationship has later been substantiated by Krumbein and Monk (1943) and Berg (1970).

Figure 2.4: (a) Cubic packing, (b) Orthorhombic packing (Graton and Fraser, 1935).

Figure 2.5: (a) Rhombohedral packing, (b) Tetragonal packing (Graton and Fraser, 1935).

Packing refers to the arrangement of grains where each grain is held in place by gravitational forces and contact with neighboring grains (Graton and Fraser, 1935). There are four basic arrangements of packing of spheres, these are cubic, orthorhombic, rhombohedral and tetragonal, as illustrated in figure 2.4 and 2.5. The enclosed void within each of the arrangements is unique. Thus, each of the fundamental packing’s has different porosities independent of sphere size as long as they are uniform. Porosities of the different packing’s are; cubic 47,6% (2.4a), orthorhombic 39,5% (2.4b), rhombohedral 26% (2.5a)

and tetragonal 30,2% (2.5b). Packing is vital for the permeability, as permeability is dependent on the porosity of the porous medium. Through a column of sand the pore throat cross sections vary considerably and it is the narrowest portion (constrictions) of the channelways that governs flow. In a porous medium, blockage of flow channels is not unusual, and it is important to note that not all porosity aid fluid flow (Fraser, 1935). A high effective (connected) porosity gives a higher permeability.

The grain size uniformity is of significant importance concerning porosity and permeability. The highest values of porosity are obtained for rocks that are perfectly sorted, while permeability vary for each unique sorting. If we consider a perfect assembly of spheres that experience addition of larger or smaller spheres, this will affect both porosity and permeability of the medium. This situation is illustrated in figure 2.6. Graton and Fraser (1935) suggest that the effect is directly proportional to the added amount. The effect of a larger sphere within an otherwise uniform assembly of spheres will influence the porosity and permeability as follows:

- The large sphere will occupy a volume that could have been filled with uniform spheres and voids for fluid transport, thus reducing porosity and permeability.
- The large sphere will create higher porosity and permeability in it's vicinity as the smaller spheres are unable to pack as closely as they would have due to the curvature of the large sphere.

So the two effects work in opposite directions for both permeability and porosity. The net result is a decrease in porosity, while the effect on permeability caused by sorting will vary for each case.

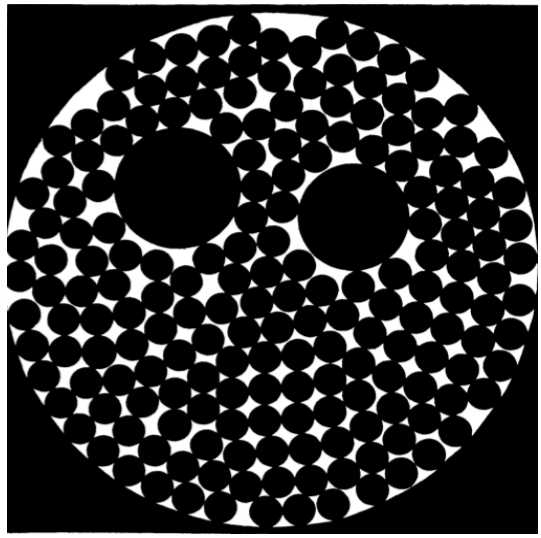

Figure 2.6: Illustrated effect of a uniform assemblage of spheres experiencing addition of larger spheres, and how this effect the surrounding pore space (Fraser, 1935).

2.11 Empirical Equations and Methods for Estimating Permeability

Since Darcy proposed his equation for flow in porous media a bunch of equations have been developed and modified based on his equation and research. Empirical factors have been added to fit observed data, while others have expressed permeability using size parameters. Below, methods for describing flow in porous media and existing equations are presented.

2.11.1 Sphere Pack Model

The sphere pack model was used in the earliest studies on flow in porous media (Fatt, 1956). This approach models the porous medium as a pack of spheres of either different or equal size, randomly or systematically distributed. Equations developed from the sphere pack model have been based on the geometrical shape of the pore space (Fatt, 1956). The disadvantages of this model are that spheres does not replicate the nature of real grains in a porous media. Thus, this model is a simplistic approximation of flow in porous media. In his paper, Fatt (1956) explains the sphere pack model to yield acceptable results when accompanied with parameters of ”*doubtful physical significance*”.

2.11.2 Bundle of Tubes

The bundle of tubes model; aim to replicate porous media by modeling flow in a collection of circular cylinders. All of the circular cylinders are of equal length, and radii occur with a frequency such that it gives the same volume probability density function as the medium (Hunt, 2014). This model account for multiphase flow, and it assumes that all tubes with radius r<A/h are filled with the wetting phase. This results from the capillary equation when there is a given solid, a pair of fluids with constant surface energy and density difference (Hunt, 2014). Where the capillary equation is given as:

$$h = \frac{2\gamma cos(\theta)}{(\rho_w - \rho_a)gr}, \tag{2.17}$$

where h is the height of rise, g the gravitational acceleration, r is the tube radius, γ the surface tension, θ the contact angle and ρ_w and ρ_a are fluid densities. The hydraulic conductivity of the fluid-filled tubes is calculated, and permeability determined (Hunt, 2014). It is worth noting that this model does not take factors as tortuosity and constrictions into consideration. Another weakness of the bundle of tubes is that it models the flow as anisotropic, although flow in porous media is known to be more or less isotropic (Fatt, 1956). Despite the bundle of tubes shortcomings it is widely applied, and Fatt (1956) states that it has been used with decent success for correlating properties of porous media.

2.11.3 Hazen - 1892

In 1892, Hazen developed an empirical equation based on grain size distribution indices, as stated in his book *The Filtration of Public Water-Supplies*, Hazen (1895). His equation was developed with the purpose to develop and design sandfilters to use in water purification and his experiments were conducted on graded sands (Carrier, 2003). The equation is one of the most used equations in the literature when determining permeability:

$$k[cm/sec] = c \cdot (D_{10})^2, \tag{2.18}$$

k is the coefficient of permeability, while, D_{10} is the grain size corresponding to 10% weighting [mm] in accordance to sieve analysis described in section 2.2. The constant, c, ranges from 0.4 to 1.2, but is usually set to 1.0.

2.11.4 Kozeny-Carman - 1937

Kozeny (1927) developed an equation including the effect of tortuosity, to account for the circuitous path for fluids through a rock and assumed that porous media could be modeled

as a bundle of streamtubes, as described in section 2.11.2. His equation is semi-empirical and is as follows:

$$k = \tau \frac{\phi^3 d^2}{(1-\phi)^2}, \tag{2.19}$$

where ϕ is the porosity, d the grain diameter, τ is the tortuosity and k is the absolute permeability. Ten years later, Carman (1937) modified Kozeny's (1927) equation, accounting for the surface irregularity of pores, yielding the more general Kozeny-Carman equation:

$$k = c_0 \tau^2 \frac{\phi^3}{S_0^2} = c_0 \tau^2 r_h^2 \phi, \tag{2.20}$$

where S_0 is the specific surface area, r_h=$\frac{\phi}{S_0}$ is the hydraulic radius and c_0 is the Kozeny constant (Carman, 1937). The Kozeny-Carman equation is widely used and gives results with reasonable accuracy.

2.11.5 Krumbein and Monk - 1942

In their paper, Krumbein and Monk (1943) analytically investigate the relation between sorting and permeability, and study the effect of size parameters on flow in porous media. Previous of their investigation others had proposed the use of parameters based on logarithmic moments. The symmetry of logarithmic plotting make these parameters ready for geometrical interpretation. In his paper, Krumbein (1936) introduces a logarithmic transformation, where traditional statistical concepts is related to logarithmic moments. It is called the Φ distribution function, and is a conversion for computational purposes.

$$\Phi = -log_2(d), \tag{2.21}$$

where d is the grain diameter in millimeters. Krumbein (1936) defines Φ as the Wentworth exponent, due to it's application to the Wentworth grade scale, which is a scale for grain size classification. Krumbein and Monk (1943) performed experiments on sand packs with porosity of 40$\pm$0.5%, an average value of 0.75 sphericity and with a roundness of approximately 0.50 (Krumbein and Monk, 1943). From their experimental data, they ended up describing permeability for an unconsolidated sand with a lognormal grain size distributions as:

$$k = 760 d^2 e^{-1.31\sigma_\Phi}, \tag{2.22}$$

where d is the diameter [mm], and σ_Φ is the standard deviation of the Φ distribution function. The equation proposed, should yield permeabilities within an acceptable accuracy for clean, well sorted and quartz rich sandstones of 30-45% porosity.

2.11.6 Berg - 1970

Berg (1970) related porosity and permeability of reservoir rocks to the primary rock properties as described in section 2.1. In his paper he highlights the importance of accounting for the different systematic packing's, and this forms the basis for his investigation. For the four different systematic packing's, as described in section 2.10, Berg (1970) expresses what he calls the rectilinear pore. This is defined as the pores that penetrates the unit cell without change in shape or direction. Where the unit cell is the smallest unit of symmetry, formed by the lines connecting the eight spheres in a packing. The rectilinear pores dimensions and numbers is unique for each packing (Berg, 1970).

By assuming that the ability for flow in porous media is mainly a function of the rectilinear pore size, Berg (1970) developed an equation. The rectilinear pore size is a function of the mean grain size, sorting, packing of the grains and the mean grain shape. When considering laminar flow through the systematic packing's a general equation was developed:

$$k = 5.1 \cdot 10^{-6} \phi^{5.1} M d^2 e^{-1.385 PD_\Phi}, \tag{2.23}$$

where ϕ is the porosity, Md is the weighted median grain size and PD_Φ is the phi percentile deviation. The equation has a narrow applicability, and yields permeabilities within an acceptable accuracy for clean sands with a porosity between 30-40%, well rounded grains and excellent sorting. This is similar applicability as with Krumbein and Monk's (1943) equation. Berg (1970) concludes that his equation should not be used as a basis for engineering calculations.

2.11.7 Katz-Thompson Relationship - 1986

Katz and Thompson (1986) proposed the following relationship for permeability of a porous media saturated with a single fluid phase:

$$k = c l_c^2 \left(\frac{\sigma_o}{\sigma_w} \right), \tag{2.24}$$

where c is a constant on the order of $\frac{1}{226}$, σ_o is the effective rock electrical conductance filled with brine, σ_w is the brine conductivity and l_c is some characteristic length of the pore space. And since $\frac{\sigma_o}{\sigma_w} = \frac{1}{F}$, we can rewrite it as:

$$k = c l_c^2 \left(\frac{1}{F} \right). \tag{2.25}$$

Katz and Thompson (1986) highlight the importance of determining the characteristic

length of the pore space. They state that the characteristic length dominates the magnitude of the permeability for porous media. Katz and Thompson (1986) determined the characteristic length for a numerous of rock samples by performing mercury injection experiments. For every step of the external applied pressure, the diameter of the pore space intruded by mercury is determined by the Young-Laplace equation for cylindrical tubes as presented in section 2.3. The pore diameters found can be plotted versus the applied pressure, and we get the characteristic mercury injection curve as seen in figure 2.7. Katz and Thompson (1986) designated the inflection point of the rapidly rising curve to be the threshold pressure p_t for the porous medium. They concluded that the pore widths l of the pores intruded at p_t satisfy $l > -4\gamma cos(\theta)/p_t$. As the early part of the intrusion curve are effects of surface defects, the characteristic length is defined by $l_c = -4cos(\theta)/p_t$.

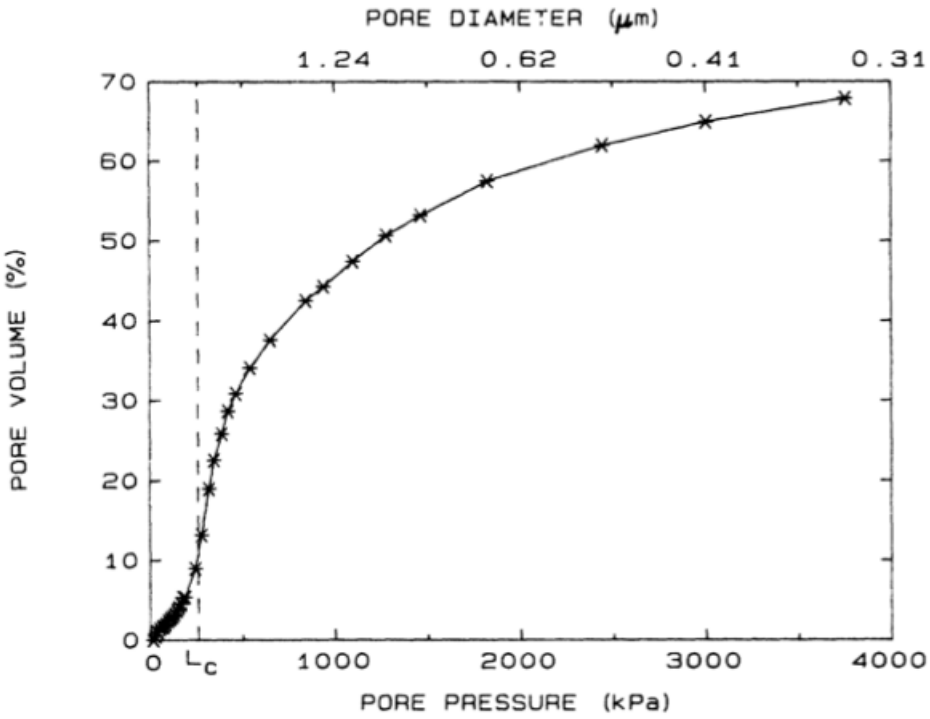

Figure 2.7: Mercury injection curve, as presented in Katz and Thompson (1986). The dashed vertical line represents threshold pressure and the characteristic length, l_c, of the pore space.

2.12 Digital Rock Technology

As we have seen there are many properties governing determination of reservoir producibility and flow in porous media. Traditionally, these properties have been determined in the lab using time-consuming methods. In recent times, the evolution of digital rock technology have made determination of these properties a lot more simple and accessible. Digital rock technology encapsulates the digitization of equipment making it possible to better understand and model rocks. Digital rock physics (DRP) is imaging and digitization of the pore space, minerals and matrix, and then numerically simulate physical processes in order to find macroscopic properties (Andrä et al., 2013). By performing high resolution imaging of the pore space, commonly a micro computed tomography (CT), and simulations providing properties as permeability, elastic-wave velocity and elastic deformation, DRP has become an industry standard (Berg et al., 2017). The available techniques offer 2D and 3D imaging of the rock and it's pore space. With the vacant image processing methods, it is also possible to do a 3D-reconstruction of 2D-images. Analysis of the images provides us with grain size distribution, irreducible water saturation, mineralogy and classification of porosity (Berg et al., 2017). From simulations one obtains relative and absolute permeability, electrical conductance, steady-state diffusion and elastic properties (Andrä et al., 2013).

2.12.1 Software

Simulations performed during this investigation have been utilizing digital rock physics, studying the properties of the pore space. This was conducted in the pore scale rock modeling software, e-Core. From simulations performed on grain size distributions, we obtained a 3D-model representing clean sand and results such as permeability and porosity. Calculation of pore area and inscribed diameter was executed in MATLAB.

The e-Core software is developed by Numerical Rocks AS, which later became Lithicon and was bought by FEI company (Field Electron and Ion Company) in 2014. The company's name is now Thermo Fisher Scientific, and has an office in Trondheim.

The software is an electronic rock core laboratory. This laboratory models petrophysical properties and simulates flow within the pore space of sedimentary rocks. The process of making a 3D numerical rock model includes the natural mechanisms of sedimentation, compaction and diagenesis.

Different sedimentation methods can be chosen, vertical and horizontal compaction applied and numerous of diagenetic processes can be mimicked. By thorough characteri-

zation of the pore network, multiphase flow can be simulated. The macroscopic transport properties such as the absolute permeability can also be calculated. This operation is CPU-intensive. Simulations in this thesis was done on a single work station, but more complex and larger systems require calculations externally on a supercomputing cluster (Numerical Rocks AS, 2012).

CHAPTER 3

THEORY

Below is the theory for the method presented in this thesis. The equations applied to express the geometrical properties of the pore area are presented, and important concepts illustrated.

3.1 Describing the Pore Throat Area Between Three Grains

Porous media constituent of sphere packs creates unique voids for the different packing's, as seen in section 2.10. The unique throats control the ability for flow in the medium, and quantification of these would improve the understanding of transport properties. There exist a number of different pore shapes in porous media, and in this thesis we have chosen to investigate triangular pore throats between grains. Assume that three spheres touch one another and are self-supported by each other, and surrounding spheres. In figure 3.1 the desired pore throat area is displayed in green. It becomes obvious that this area can be expressed as the area of the triangle formed by the grain centers, minus the red circle sectors of each grain. This is better displayed in figure 3.2.

The first step of describing the pore throat area was to express the angles α, β and γ. As we only know the sides of the triangle we used the law of cosine for expressing the angles. This resulted in the following expressions:

$$\alpha = cos^{-1}\left(\frac{(r_1+r_2)^2+(r_1+r_3)^2-(r_3+r_2)^2}{2\cdot(r_1+r_2)\cdot(r_1+r_3)}\right), \tag{3.1}$$

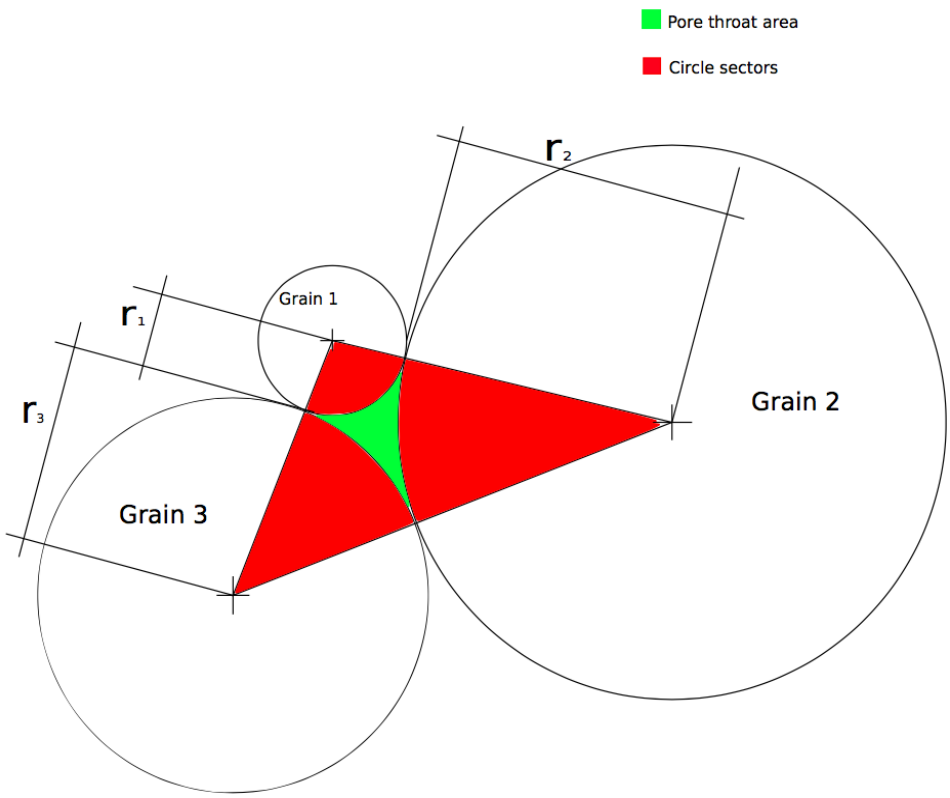

Figure 3.1: Sketch displaying three circles, representing grains, creating the pore throat area (as seen in green).

$$\beta = cos^{-1}\left(\frac{(r_1 + r_2)^2 + (r_3 + r_2)^2 - (r_1 + r_3)^2}{2 \cdot (r_1 + r_2) \cdot (r_3 + r_2)}\right), \tag{3.2}$$

$$\gamma = cos^{-1}\left(\frac{(r_1 + r_3)^2 + (r_3 + r_2)^2 - (r_1 + r_2)^2}{2 \cdot (r_1 + r_3) \cdot (r_3 + r_2)}\right). \tag{3.3}$$

As it was desirable to find the area of the triangle, we needed to express the height of the triangle. This was done by simple trigonometry, and the height was expressed as:

$$h = (r_1 + r_3) \cdot sin(\gamma). \tag{3.4}$$

Thus, the area of the triangle is:

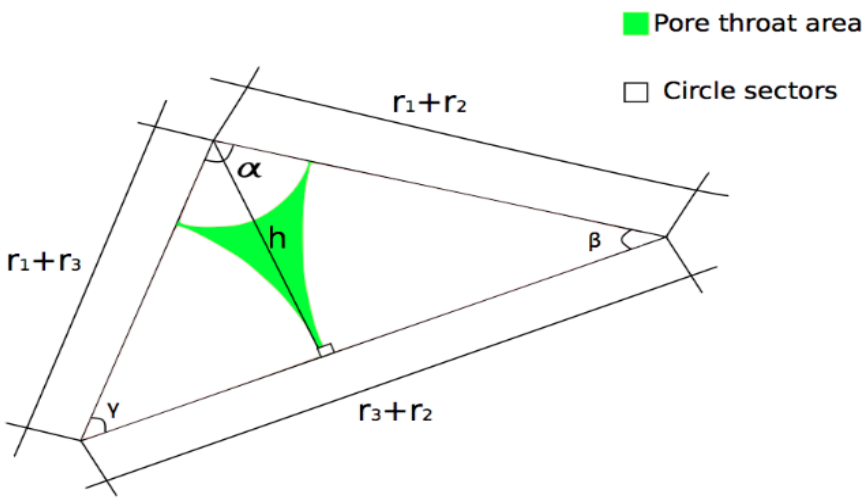

Figure 3.2: Circle sectors of the three grains and the resulting pore area.

$$A_{triangle} = \frac{1}{2} \cdot b \cdot h = \frac{1}{2} \cdot (r_3 + r_2) \cdot (r_1 + r_3) \cdot sin(\gamma). \tag{3.5}$$

To get the pore throat area one must subtract the area of the three circle sectors from $A_{triangle}$. The circle sectors can be expressed as follows:

$$S_i = \pi \cdot r_i^2 \cdot \frac{\theta}{2\pi} = \frac{r_i^2 \theta}{2}, \tag{3.6}$$

such that:

$$S_1 = \frac{r_1^2 \cdot \alpha}{2}, \quad S_2 = \frac{r_2^2 \cdot \beta}{2}, \quad S_3 = \frac{r_3^2 \cdot \gamma}{2}. \tag{3.7}$$

The area of the pore throat can thus be expressed as:

$$A_{pore\ throat} = A_{triangle} - S_1 - S_2 - S_3. \tag{3.8}$$

3.2 Finding the Inscribed Radius

The inscribed radius of the black grain seen in figure 3.3 can be expressed using Descartes' theorem, also known as the kissing circle theorem. Soddy (1936) generalized this in his

poem, "*The Kiss Precise*", as can be seen in appendix D. This theorem describes the configuration of four mutually tangent circles where three of the circles have a common tangent circle (Lagarias et al., 2002). This situation corresponds to that in figure 3.3. The radii of the circles are r_1, r_2, r_3 and r_{insc}. Thus, the curvature of the circles can be written as $k_i = \frac{1}{r_i}$. From the theorem a quadratic equation is provided. When solved, it determines the possible values for the radius of the fourth circle tangent, in this case the inscribed radius. In a Descartes configuration of four mutually tangent circles, the curvatures satisfy:

$$\sum_{i=1}^{4} k_i^2 = \frac{1}{2}\left(\sum_{i=1}^{4} k_i\right)^2, \tag{3.9}$$

thus, with regard to figure 3.3, we can write:

$$k_1 = \frac{1}{r_1}, \quad k_2 = \frac{1}{r_2}, \quad k_3 = \frac{1}{r_3}, \quad k_{\text{insc}} = \frac{1}{r_{\text{insc}}}, \tag{3.10}$$

with this defined , we can state Descartes theorem as:

$$(k_1 + k_2 + k_3 + k_4)^2 = 2\,(k_1^2 + k_2^2 + k_3^2 + k_4^2). \tag{3.11}$$

From this, one can solve for the inscribed radius, r_{insc}, resulting in the following expression:

$$r_{\text{insc}} = \frac{1}{k_1 + k_2 + k_3 \pm 2 \cdot \sqrt{k_1 \cdot k_2 + k_2 \cdot k_3 + k_3 \cdot k_1}}. \tag{3.12}$$

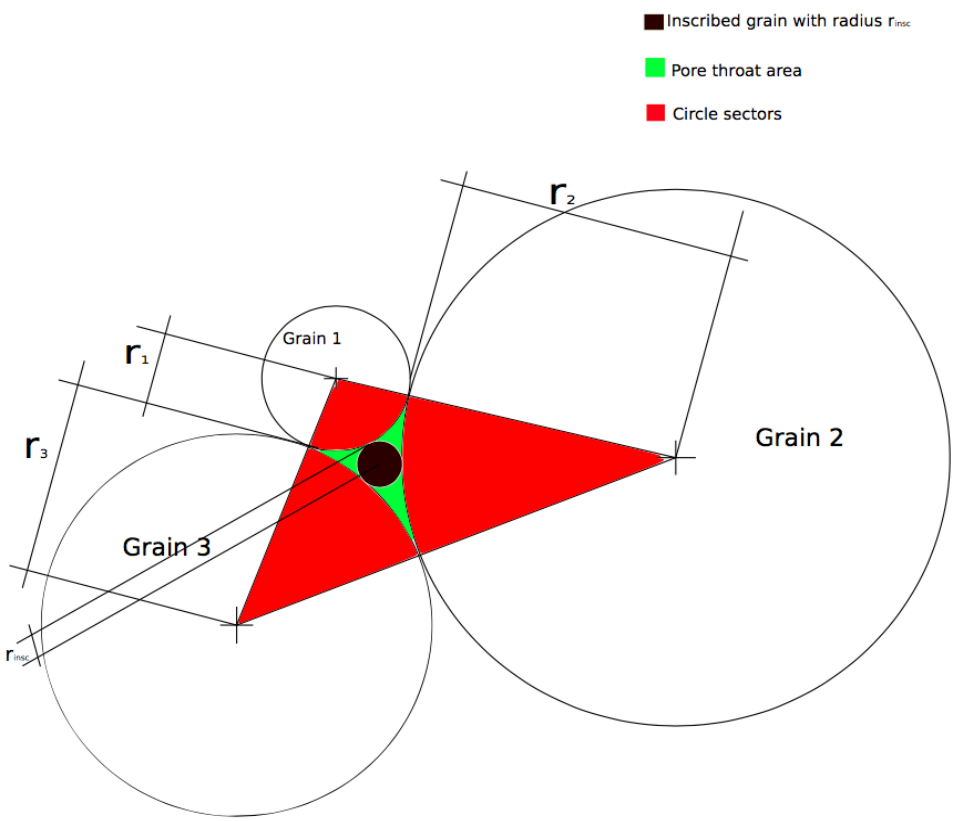

Figure 3.3: Visual representation of the pore area with an inscribed grain, with radius r_{insc}

CHAPTER 4
METHODOLOGY

In the following chapter the methodology used in this thesis is presented. Calculations and experimental work performed is described and illustrated.

4.1 Generating Sphere Packs Using e-Core

As this thesis aims to investigate the relation between a grain size distribution and transport properties, classical sandstones was studied in order to get an overview of typical properties. One of the sandstones that is typically studied regarding transport properties is the Fontainebleau sandstone. A micro-CT image of a Fontainebleau sandstone, obtained from Digital Rocks Portal (Berg, 2017), was imported into e-Core. The imported CT-image provided a 3D-model of the rock as illustrated in figure 4.1. By using grain recognition, the grain size distribution was extracted. From the grain size distribution the mean and standard deviation (non VW) was found to be μ = 148,9 $\approx$ 150μm and σ = 36,7 $\approx$ 40. These values represent a fairly clean; quartz rich and well sorted sandstone, and was used as basis for the generation of sphere packs.

4.1.1 Volume-Weighting Grain Size Distribution

In section 2.12.1, the e-Core software used in this thesis is presented. e-Core offers different distribution models; Min-Max distribution, Normal distribution and Existing distribution. The normal distribution was used for the first simulations. In addition to using this embedded model, existing distribution model was used. This model utilizes an existing grain size distribution. For this purpose an ascii file is needed. Hence, such a file must be

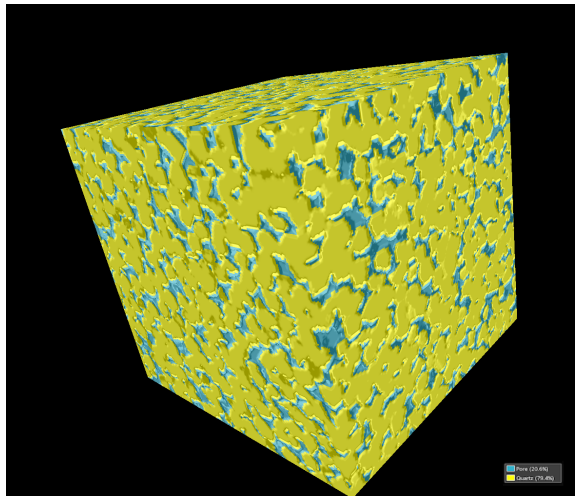

Figure 4.1: 3D-model view of the Fontainebleau sandstone. Side lengths of 2500μm and voxels of 5μm

generated. This was done using Excel as described below.

By defining a value for mean grain size and standard deviation a volume weighting of the distribution was pursued. From these values a maximum and minimum grain size was determined as $\mu \pm 2\sigma$. Number of bins was chosen to be 100. A list of grain sizes was then generated based on the input values. The grain sizes were then distributed according to the cumulative distribution function. From the CDF, the distribution was represented volume wise. With the volumes, the number of grains per bin size could be found. Thus, creating a volume weighted grain size distribution.

A script was made for transforming the distribution from Excel to a readable format for e-Core. The script can be seen in Appendix A.1.

4.1.2 Simulation Process

As mentioned, e-Core offers three different grain size distributions. For the simulations the existing distribution was chosen. For generating these distributions we chose to determine a set of parameters. These were: mean grain size, standard deviation, minimum grain size and maximum grain size.

For the simulations, five mean grain size values and standard deviations was chosen to generate a representative distribution similar to the Fontainebleau sandstone. The mean

grain sizes are varied between 150-250μm. For each mean grain size the standard deviation is varied between 15-75. Minimum and maximum grain size was defined to be $\mu \pm 2\sigma$. The complete simulation set up can be seen in table B.1 in appendix B.

Before starting the simulations, a set of configurations must be set. The first configuration to be determined is the model type. e-Core offers different model types that mimic distinct deposition styles. For the simulation the laminated model was chosen. The simulation set up above includes only a single lamina. The number of grid cells (x) was chosen to be 500, while the grid cell size was set to 5 μm. The grid cell size was chosen based on the desire of having 5-10 grid cells per grain, as the smallest grains approach 25μm. Further, grain bed properties must be determined. In e-Core, four common parameters defining the grain bed composition was configured. These parameters were; amount of elliptical grains, maximum sphericity factor, amount of feldspars and amount of unsolvable feldspars. The values was set to, 0%, 1.0, 0% and 0%, respectively.

4.2 Generating an Equation Based on Mean Grain Size and Standard Deviation

With all properties set as described in the previous section, the created grain size distributions from Excel was imported into e-Core and sedimentation of the sphere packs was conducted. After the sedimentation, flow simulations was performed in order to obtain absolute permeability for each sand pack. All parameters were kept at default for the flow simulations. The flow simulation computes absolute permeability using the Lattice Boltzmann method. With the acquired absolute permeabilities from e-Core, an equation using statistical properties of grain size distributions was pursued using the solver package in Excel. Plots of acquired properties from flow simulations served as a tool for investigating relationships and dependencies.

4.3 Calculating Pore Area and Approximating Permeability

As earlier described the major ambition of this thesis is to express the transport properties using the pore area constructed by three tangent circles, where the circles is a 2D cross section of grains. For calculating the pore area, the theory presented in section 3.1 served as basis. The calculation requires three grains. These three grains was randomly picked from the grain size distribution. This would create a realistic void space constituent of

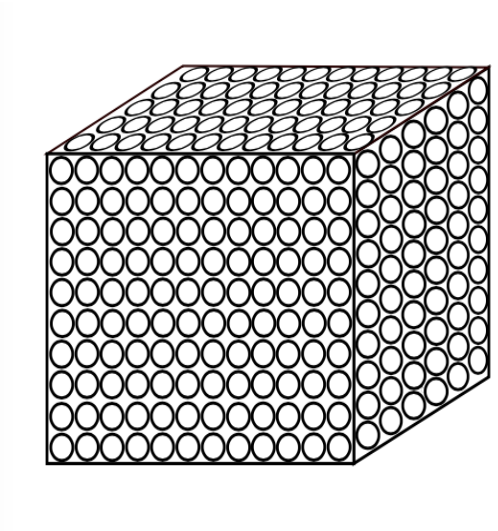

Figure 4.2: Visualization of a cube with spheres.

three independently chosen grain sizes. Calculating the pore area of a representative number of grain constellations would give a useful approximation of flow potential. The mean grain sizes and standard deviations that served as basis for generating the sphere packs can be viewed in appendix B, table B.1, but this time the smallest grain size, 150μm, was not included. Modeling and visualization was performed in e-Core, while calculations was performed in MATLAB. The MATLAB code is presented in appendix A.2 and A.3.

The first approach of utilizing pore area as a descriptor of permeability was based on grain size distribution properties and flow and computational simulations in e-Core and MATLAB, respectively. Flow simulations in e-Core were performed on a cubic system. If we consider one of the sides of this cube, there will be a certain area that would permit flow as visualized in figure 4.2. This area equals the porosity. Mean grain size and lengths of the system served as estimation on the number of pore throats.

$$n_{\text{throats}} = \frac{\text{System Length}}{\text{Mean Grain Size}}, \tag{4.1}$$

thus, the total number of throats in a cube is n^3_{throats}. Each of the pore throats contributes to the total fluid transport and has conductivity, g, dependent on the pore area. The conductivity of each throat can be calculated using equation 2.9 as seen in section 2.5, resulting in a set of conductivities. In equation 2.9 the length, l, is put to be the mean grain size diameter, l_{mean}, such that:

$$g = \frac{A^2}{8 \cdot \pi \cdot l_{\text{mean}}}. \tag{4.2}$$

The conductivity was calculated for each throat and for each layer (i.e a horizontal slice with a height equal to the radius) the harmonic mean was calculated. Total conductivity was found by summing up the conductivity for each of these layers. This conductivity calculation is shown in appendix A.4. With the conductivity known, one can use the Darcy equation to express and calculate the permeability.

$$k = \frac{\sum g}{l_{\text{sys}}}, \tag{4.3}$$

where l_{sys} is the length of the simulated system. This procedure gives an approximate permeability value and was performed for the pore area and the inscribed grain area.

The calculation of the inscribed grain diameter, as seen in section 3.2, was performed with a random choosing of three grains from a grain size distribution. Using the randi function in MATLAB, generating n^3 number of constellations of three random grains and calculating the inscribed diameter of each. This gives a representative number of pore throats for calculating the mean inscribed diameter. The MATLAB-codes performing these operations can be seen in appendix A.6. With conductivities for the different approaches, an equation was pursued using the solver package in Excel.

4.4 Implementing Shape Factor

The implementation of a shape factor is to account for angular pores. As the Hagen-Poiseuille equation is valid for cylindrical pipes, a factor to replicate and represent the essential features of a pore space would make it more suitable for natural porous media. By the definition of Øren et al. (1998), the shape factor for a cylinder becomes:

$$G = \frac{A}{s^2} = \frac{\pi r^2}{(2\pi r)^2} = \frac{1}{4\pi}. \tag{4.4}$$

For triangular pores Øren et al. (1998) defined the shape factor as seen in equation 2.11. The length in the denominator is now the mean grain size, and we write:

$$K = \frac{3}{5}\frac{A^2 G}{l_{\text{mean}}}. \tag{4.5}$$

With the shape factor implemented, the permeability was calculated in the same manner as above. The conductivity calculation with shape factor can be seen in appendix A.5.

4.5 Pursuing Permeability Using Katz-Thompsons Relationship

In the process of investigating properties of the pore area and their relation to permeability, Katz and Thompson's (1986) relationship, as described in section 2.11.7, was studied. Katz-Thompson relationship utilizes mercury intrusion experiments for defining the characteristic length of the pore space. With no data on this, other characteristic lengths of the pore space were pursued, such as pore diameter. These were tried using trial and error. In addition to this, some adjustment to the constant was necessary.

4.6 Expected Diameter

Descartes theorem as described in equation 3.11 was used to find the expected value of the inscribed diameter. We can start with the expected value of the complete expression and simplify:

$$d_{insc} = E\left(\frac{2}{k_1 + k_2 + k_3 \pm 2 \cdot \sqrt{k_1 \cdot k_2 + k_2 \cdot k_3 + k_3 \cdot k_1}}\right), \tag{4.6}$$

note that the numerator is multiplied with two to get the diameter. This expression can now be simplified and broken up. Lets focus on the denominator:

$$E\left(\frac{1}{r_1} + \frac{1}{r_2} + \frac{1}{r_3} + 2 \cdot \sqrt{\frac{1}{r_1} \cdot \frac{1}{r_2} + \frac{1}{r_2} \cdot \frac{1}{r_3} + \frac{1}{r_1} \cdot \frac{1}{r_3}}\right), \tag{4.7}$$

which can be further simplified to:

$$E\left(\frac{1}{r_1}\right) + E\left(\frac{1}{r_2}\right) + E\left(\frac{1}{r_3}\right) + 2 \cdot E\left(\sqrt{\frac{1}{r_1} \cdot \frac{1}{r_2} + \frac{1}{r_2} \cdot \frac{1}{r_3} + \frac{1}{r_1} \cdot \frac{1}{r_3}}\right). \tag{4.8}$$

For the denominator we end up with:

$$\begin{aligned} \Rightarrow 3 \cdot E\left(\frac{1}{X}\right) + 2 \cdot \left(\sqrt{\frac{1}{X^2}}\right) &= 3 \cdot E\left(\frac{1}{X}\right) + 2\sqrt{3} \cdot E\left(\sqrt{\frac{1}{X^2}}\right) \\ &\simeq (3 + 2\sqrt{3}) \cdot E\left(\frac{1}{X}\right). \end{aligned} \tag{4.9}$$

The expected value for the inscribed diameter can thus be expressed as:

$$d_{insc} = \frac{2}{(3 + 2\sqrt{3}) \cdot E\left(\frac{1}{X}\right)}. \tag{4.10}$$

It is worth noting that between equation 4.8 and 4.9 the denominators are changed from radius to a common X. This is a valid assumption as the radii are gathered from the same distribution and is thus interchangeable. The computation of the expected value for the inscribed radius was done in MATLAB and is presented in appendix A.7.

In the same manner as before, we can develop a relationship based on the expected diameter and the variance of the mean inscribed diameters. A best-fit equation was developed using the solver package in Excel.

CHAPTER 5

RESULTS

Characteristics from a grain size distribution and how they can be applied in describing transport properties of porous media are investigated. The equations developed are presented along with supporting figures. Lastly, the equations validity and application is depicted.

5.1 Volume Weighting

The first sets of sphere packs generated in e-Core based on the default normal distribution provided a grain size distribution as can be seen as the black curve in figure 5.1. e-Core provides a cumulative distribution of the grains that is weighted by number. Thus, it yields a rock where there is very few of the smaller grains compared to larger grains volume wise. Performing a volume weighting on the distribution results in a distribution constituent of a higher number of small grains compared to larger ones. In figure 5.1 the volume-weighted distribution is represented by the blue curve. A volume-weighted distribution is viewed as more representative of a realistic rock because the ratio of small to large grains is better characterized. The higher amount of small grains has two main effects. Firstly, porosity will decrease due to the occupation of pore space by small grains in between larger ones. Secondly, the presence of fine-grained material in pore throats will decrease the rocks ability for flow.

One of the indicators supporting a volume-weighted distribution was the effect of standard deviation on porosity. In table 5.1, the effect can be studied. Initially, with the non-volume

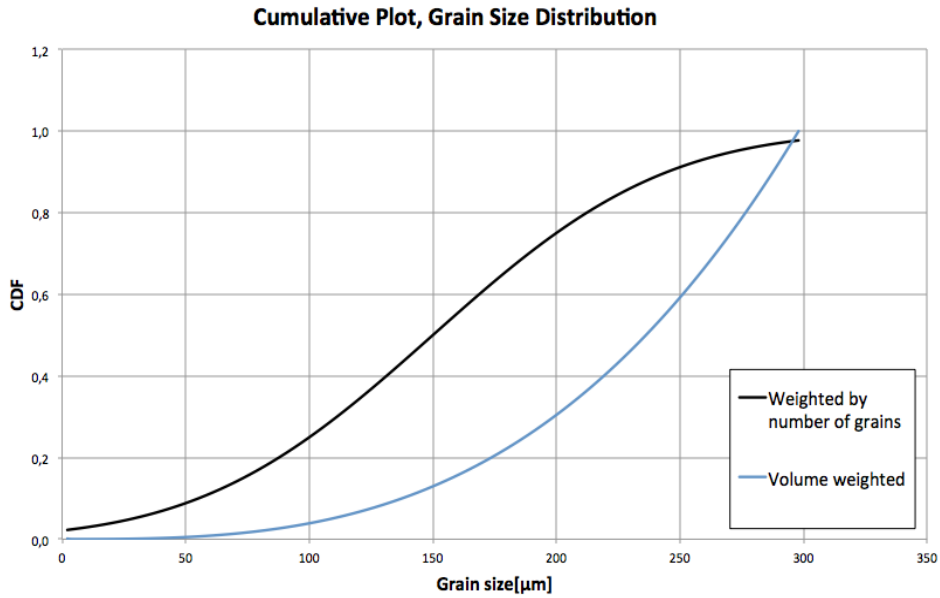

Figure 5.1: Cumulative plot showing grain size distribution weighted by number of grains versus volume weighted. The volume weighted distribution has a higher amount of small grains compared to the non volume weighted.

Case	MGS(μ)	SD(σ)	ϕ(not VW)[%]	ϕ(VW)[%]	k(not VW)[mD]	k(VW)[mD]
1	175	25	39.05	39.27	29407	30436
2	175	50	38.13	36.26	35278	18523
3	175	75	37.77	33.83	44967	14651

Table 5.1: Study on the effect of standard deviation on porosity and permeability.

weighted (VW) distribution the porosity decreases slightly when standard deviation is increased, while the permeability increases with increasing standard deviation. Thus, we have a coarse medium, where the porosity is decreasing, but lack of small grains gives rise to increasing permeability.

5.2 Equation Based on Mean Grain Size and Standard Deviation

As seen earlier, there have been proposed a multiple of equations describing flow in porous media. A common feature for all of these equations have been the diameter squared multiplied with porosity relation. Hazen (1895) was one of the earliest describing flow using

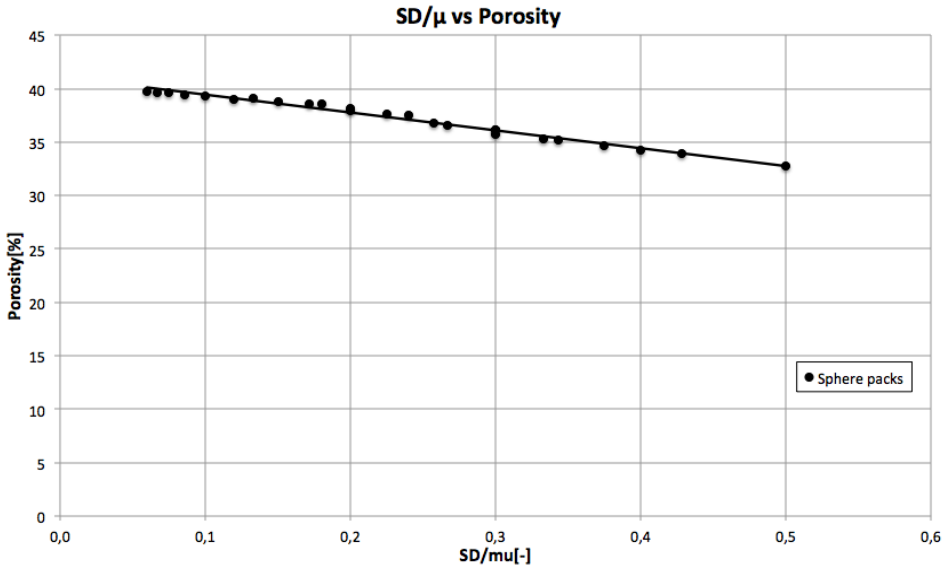

Figure 5.2: Porosity plotted against the coefficient of variation, showing a linear relationship.

this relation. Later, Krumbein and Monk (1943) and others proposed equations utilizing this relation. Thus, it is meaningful to start with this relation and develop further:

$$k = R \cdot \phi\mu^2, \tag{5.1}$$

here R is a constant that includes properties affecting flow, and will be described later. After studying the graph, figure 5.2, effect of mean grain size and standard deviation on porosity, it became clear that porosity could be described as a linear function of the coefficient of variation. Also worth noting from figure 5.2 is that zero standard deviation gives a porosity of 41.125. This sounds plausible as Graton and Fraser (1935) concluded that a cubic packing of spheres yields a porosity of 47.6%. We can write the equation as:

$$k = R \cdot \mu^2 \cdot \left[a \cdot \left(\frac{\sigma}{\mu}\right) + b\right] = R \cdot (a\mu\sigma + b\mu^2). \tag{5.2}$$

Further, the equation was developed by relating R to mean grain size and standard deviation. This was done by plotting $\frac{\sigma}{\mu}$ against $\frac{k}{\mu^2\phi}$, see figure 5.3. By employing linear regression, the equation is written as:

$$k = \left[a\mu\sigma + b\mu^2\right] \cdot \left[c\left(\frac{\sigma}{\mu}\right) + d\right]. \tag{5.3}$$

The constants a, b, c and d is extracted from the linear regression seen in figure 5.2 and

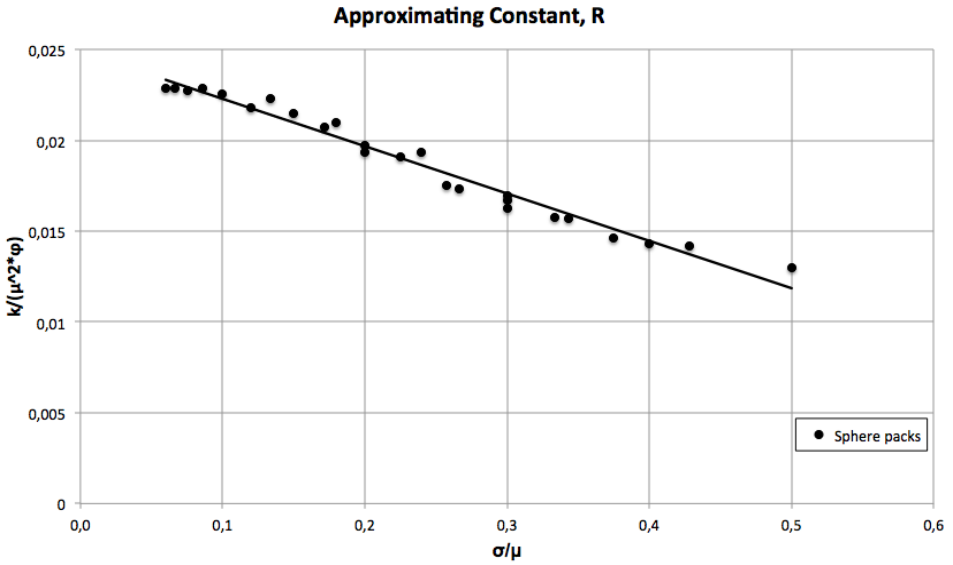

Figure 5.3: A linear representation approximating the constant, R.

5.3. The equation from linear approximation for the porosity and R are respectively:

$$\phi = -16.733 \cdot \left(\frac{\sigma}{\mu}\right) + 41.125, \tag{5.4}$$

$$\frac{k}{\mu^2\phi} = -0.0261 \cdot \left(\frac{\sigma}{\mu}\right) + 0.0249, \tag{5.5}$$

yielding the final equation based on the simulation set up in table B.1:

$$0.4367 \cdot \sigma^2 + \mu \cdot (1.024\mu - 0.4167\sigma - 1.073). \tag{5.6}$$

5.3 Equation Based on Pore Area

The idea of the second approach was similar to the first approach, but properties of the pore area were chosen as basis for expressing the permeability. The theory that serves as a basis for the results presented can be found in chapter 3. Also, chapter 4 describes the procedure and idea of the calculation.

First, the conductivity of the whole pore area was investigated and permeability calculated as described in section 4.3. Secondly, the pore area with the included shape factor as

described in section 2.6 and 4.4 was calculated. From the obtained conductivities, permeability was calculated using Hagen-Poiseuilles equation as described in section 2.4. The results of this calculation can be seen in figure 5.4 and 5.5. These plots show that these two approaches is overestimating the permeability of the sphere packs. Another aspect worth noting is the apparent decrease in permeability when the shape factor proposed by Øren et al. (1998) is implemented.

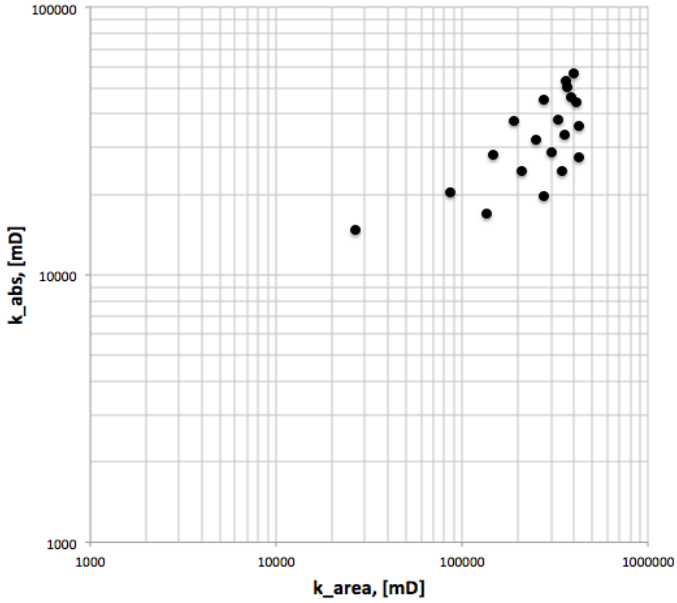

Figure 5.4: Permeability calculated from raw pore area as expressed in section 3.1.

It became clear that using the raw pore area or in combination with the shape factor provided permeabilities higher than the actual values. After this the mean inscribed pore diameter as presented in section 3.2 was investigated and conductivities calculated. The obtained permeabilities found from this approach are presented in figure 5.6. When comparing figure 5.4 and 5.5 to figure 5.6, the method using mean inscribed pore diameter estimate permeabilities closest to those obtained from e-Core. Based on these results it was chosen to further investigate and develop a relationship for the approach using the mean inscribed diameter of the pore area.

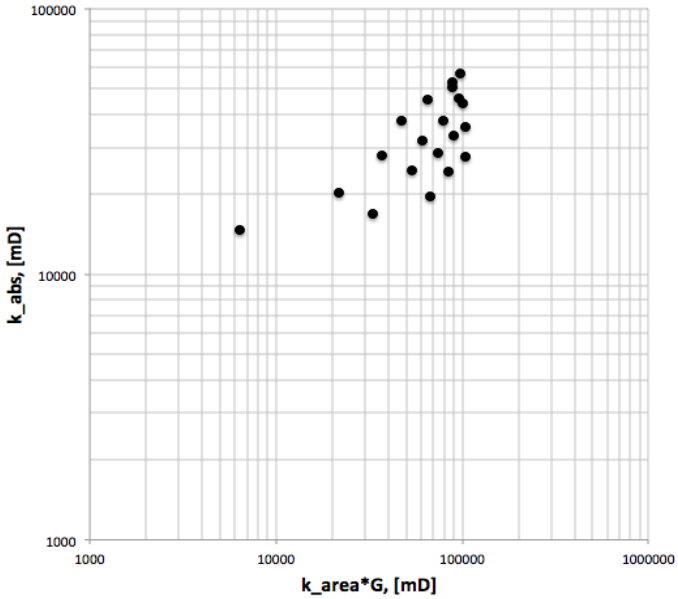

Figure 5.5: Permeability calculated from raw pore area with implemented shape factor. This is described in section 2.6 and 4.4.

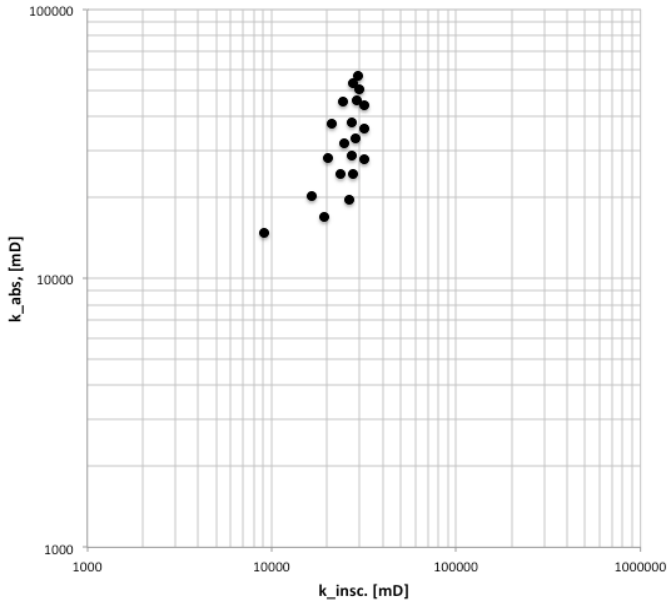

Figure 5.6: Permeability calculated from inscribed diameter as illustrated in figure 3.3.

5.4 Katz-Thompson Relationship Investigated

As mentioned in section 4.5, the Katz-Thompson relationship was studied in the process of developing an equation using pore area characteristics. Katz and Thompson (1986) relationship uses a characteristic length of the pore space, as is described in detail in section 2.11.7. This length was determined from mercury injection experiments, and as this was not available for the sphere packs in question, other characteristic lengths of the pore area was pursued. Using the mean inscribed pore diameter of a data set, as described in section 4.3, and changing Katz and Thompson's (1986) proposed constant from $\frac{1}{226}$ to $\frac{17}{100}$. Using another measure for the characteristic length will understandably affect the pre-factor c in the Katz-Thompson's equation. We obtained the resulting values shown in figure 5.7.

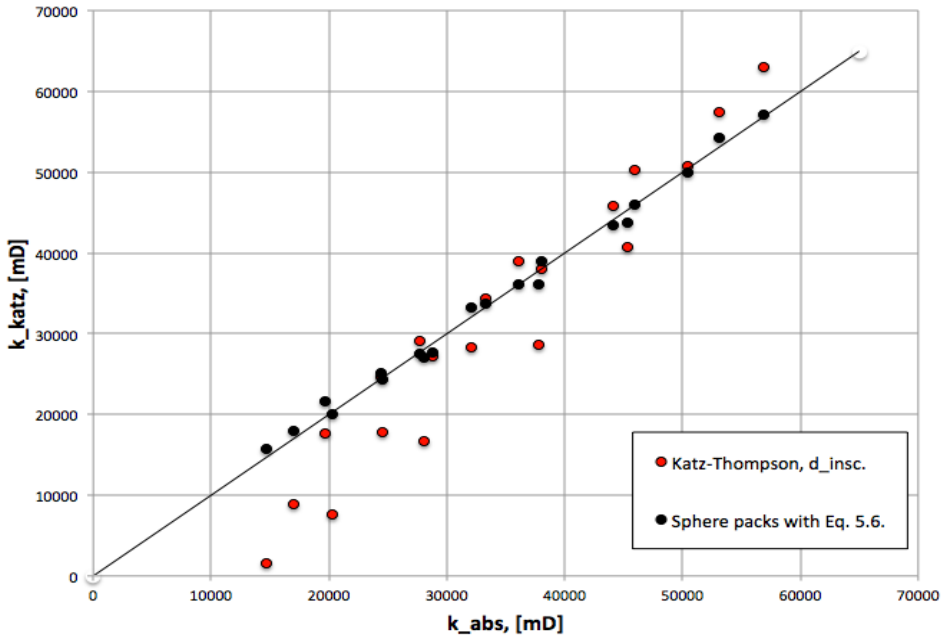

Figure 5.7: Katz-Thompson relationship tested on the sphere packs. It estimates permeabilities with some accuracy, but underestimates permeability for the packs with lowest initial permeability.

From the plot, we see that Katz and Thompson's (1986) relationship estimate permeabilities with a decent accuracy. The packs that have an initial low permeability is underestimated using this relationship. Although this plot shows some misalignment, there seem to be a relation between the mean inscribed pore diameter and permeability. This observation further substantiates a pursue of an equation using the mean inscribed pore diameter from a grain size distribution.

5.5 Further Investigation of Area of Inscribed Diameter

As we saw from section 5.3 and 5.4 there was indications that the mean inscribed pore diameter provided permeabilities with the highest accuracy. This support a pursue of relating inscribed pore diameter to transport properties of porous media. The mean inscribed diameter was found using the method described in section 4.3. This diameter will vary around a short interval for each data set due to the randomizing of the calculation. With a value of the mean inscribed diameter in combination with the variance of the randomized inscribed diameters, one has two useful values. These two values were found for each combination presented in table B.1. Based on these two values one is able to develop a meaningful relationship with permeability. This was done using the Excel add-in, solver.xlam, in combination with plotting. After performing optimization using the solver in Excel, we end up with the following equation:

$$k[mD] = 35.89 \cdot d_{insc}^2 + 5491.6 \cdot \left(\frac{\sigma}{d_{insc}}\right)^{0.95}, \tag{5.7}$$

where d_{insc} [μm] is the average inscribed diameter and σ is the variance of the inscribed diameters. The constants in the equation are found after tuning the equation using Excel. The standard deviation of data must be seen in context with the mean of the data; hence the use of the coefficient of variation, as this describes the dispersion of the probability function.

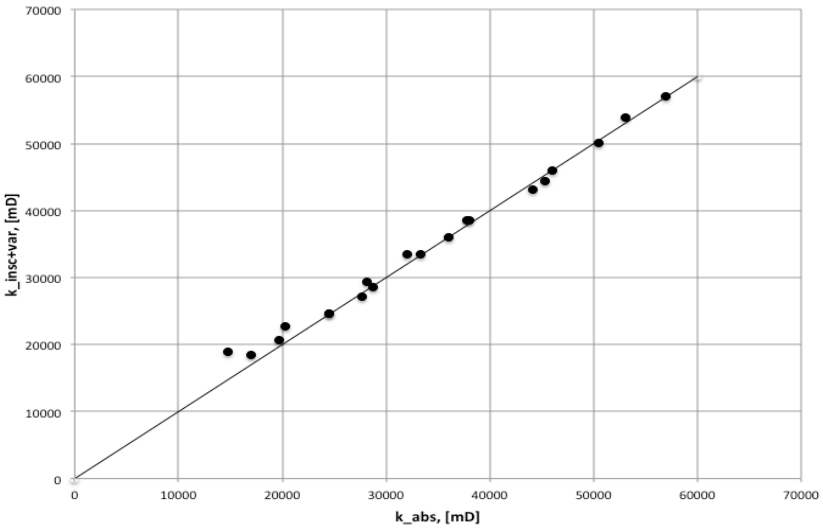

Figure 5.8: Permeability calculated from equation 5.7 plotted versus absolute permeability from e-Core.

5.6 Expected Inscribed Diameter

Equation 5.7 requires the use of the randomizer as presented in appendix A.6.2. The randomizer, in combination with the script in appendix A.6.3, finds the mean inscribed diameter, d_{insc}, and the variance, σ. It would have been desirable to express both d_{insc} and σ as expected values without the need of the randomizer. The expected value of d_{insc} was expressed using statistical procedure as is outlined in section 4.6. The expected value of the variance proved to be complex and not feasible. Although, we are now able to express the expected inscribed diameter without the randomizer, the variance still requires the use of it. In figure 5.9 the expected inscribed diameter is plotted versus the actual calculated mean inscribed diameter for each sphere pack and it shows that it predicts the inscribed diameter to a satisfactory degree.

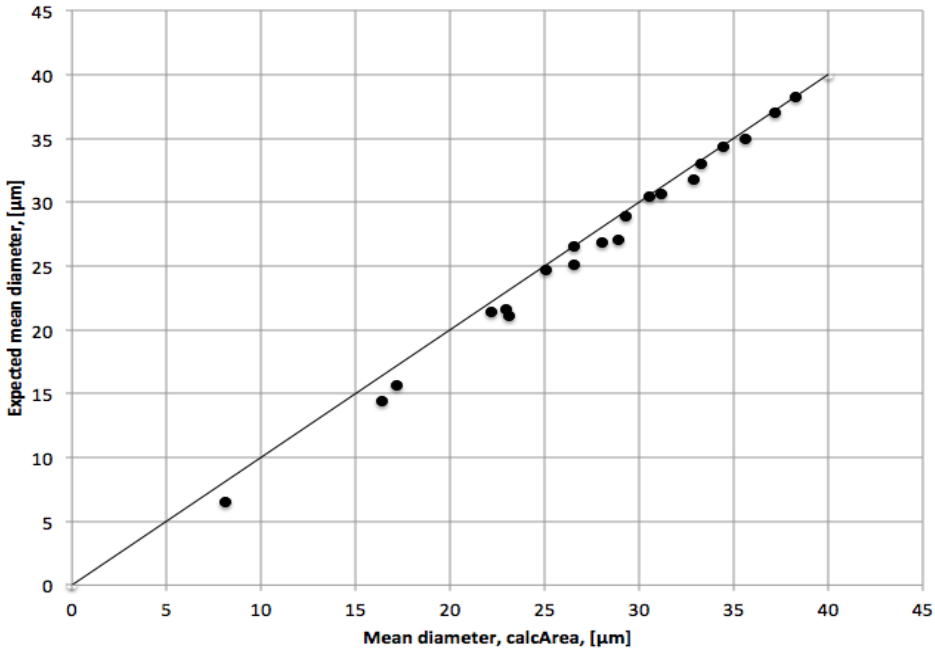

Figure 5.9: The actual mean diameter plotted versus the expected value. There are some discrepancies for the smallest diameters and a general trend of slightly smaller diameters from the expected value compared to the actual.

Figure 5.10 and 5.11 substantiates the use of the expected inscribed diameter and it's variance. As can be seen, the inscribed expected diameter converges and shows limiting behavior. The same apply to the variance. This was reassuring as we could say that both expected inscribed diameter and the variance of the mean inscribed diameters converges as number of grains increase.

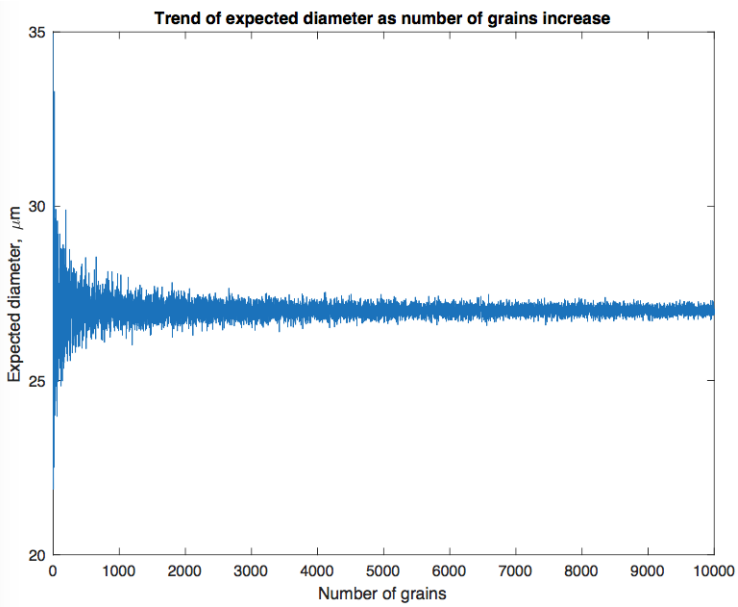

Figure 5.10: Expected inscribed diameter converging as number of grains increase.

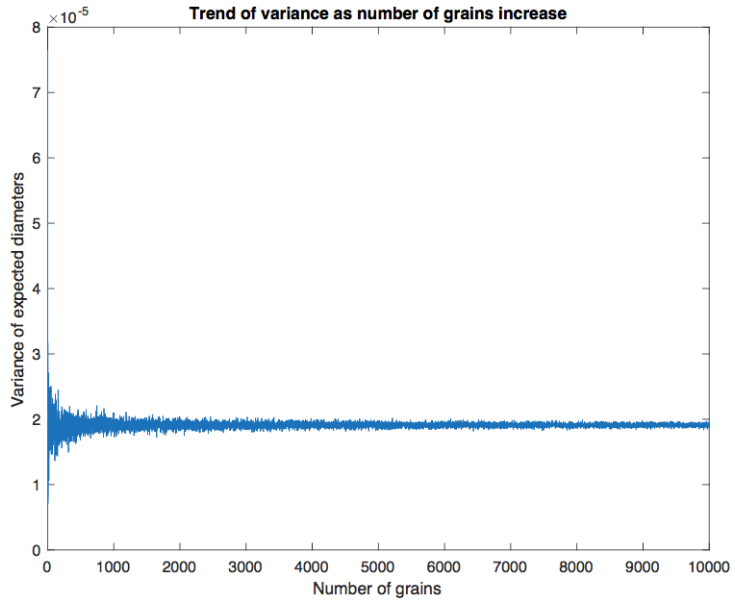

Figure 5.11: Variance of the expected inscribed diameter converging as number of grains increase.

With the expected inscribed diameter and variance known, we can perform iterations and optimization in the same manner as described earlier. This results in the following equation:

$$k[mD] = 36 \cdot d_{exp}^{2.02} + 5491.1 \cdot \left(\frac{\sigma}{d_{exp}}\right)^{0.945}, \tag{5.8}$$

where d_{exp} [μm] is the expected inscribed diameter. In SI-units the equation becomes:

$$k[m^2] = (4.88\text{E-}2) \cdot d_{exp}^{2.02} + (2.61\text{E-}6) \cdot \left(\frac{\sigma}{d_{exp}}\right)^{0.945}, \tag{5.9}$$

where the expected inscribed diameter, d_{exp} [m], now is metric.

5.7 Formula Applied to Sand Packs

For testing the equation presented above, equation 5.9, a few sand packs was acquired from Imperial College London (2017). Sand packs resemble sphere packs, but texture effects such as sorting, packing, grain size, shape and orientation are more prominent. The preliminary tests showed that equation 5.9 overestimated permeability for these sand packs as can be seen in figure 5.12. It is believed that a combination of texture properties affect the permeability estimation. A pre-factor was added to the equation to reduce the permeability closer to the actual value of the sand packs. This factor was found using manual optimization in Excel, and was determined to be:

$$c = 0.57$$

.

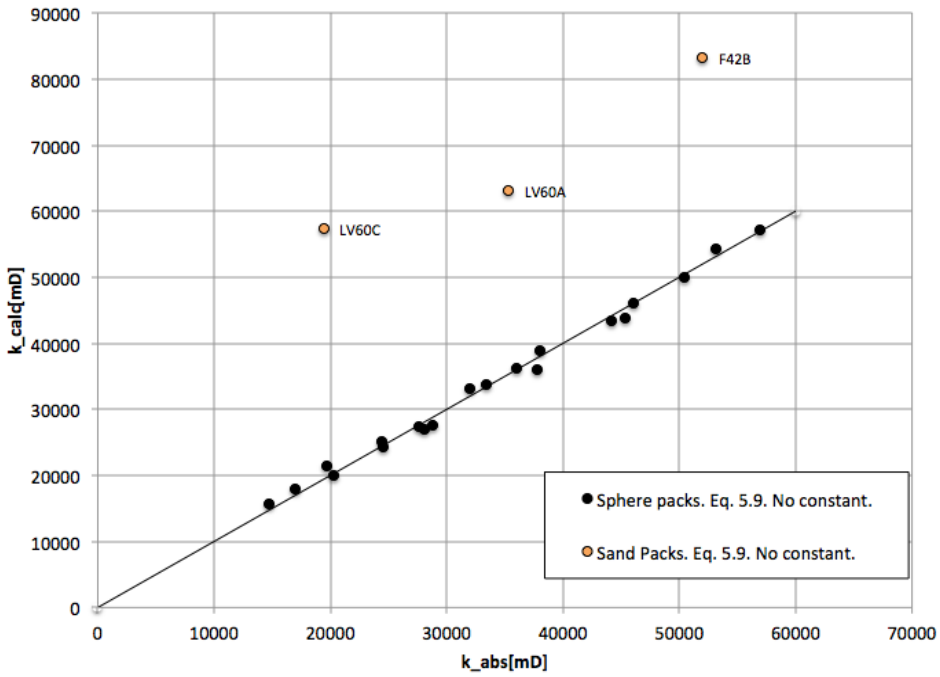

Figure 5.12: Preliminary test of equation 5.9 on three sand packs from Imperial College London (2017), LV60C LV60A and F42B.

5.8 Final Equation and it's Validity

With the pre-factor found in section 5.7, we end up with the final equation:

$$k = c \cdot \left[(4.88\text{E-}2) \cdot d_{exp}^{2.02} + (2.61\text{E-}6) \cdot \left(\frac{\sigma}{d_{exp}} \right)^{0.945} \right], \tag{5.10}$$

where:
k = permeability [m^2]
c = 0.57, a pre-factor adjusting for the overestimation of permeability on sand packs
d_{exp} = expected inscribed diameter [m]
σ = variance
The equation is based on a clean sphere pack of good sorting, clean quartz with no feldspars and a high-energy sedimentation. Hence, the constant c is restricted to use on sand packs and other sandstones.

The precision of equation 5.6, 5.9 and 5.10 can be seen in figure 5.13. The black dots

represent the simulated sphere packs as described in section 4.1.2 and in appendix B, table B.1. These are clearly linearly distributed as the equation was developed with these as a basis. Further, we see that equation 5.6 based on mean grain size and standard deviation and equation 5.9 based on expected inscribed diameter closely match each other. Although, matching each other they are quite inaccurate overestimating the permeability by a factor of two to three. Also, the equation based on expected inscribed diameter is slightly more off than equation 5.6. With the included pre-factor, c, as described in section 5.7, the permeability is considerably closer to the actual permeability. This indicates that a factor should be added to the equation when applied to actual porous media, such as sand packs.

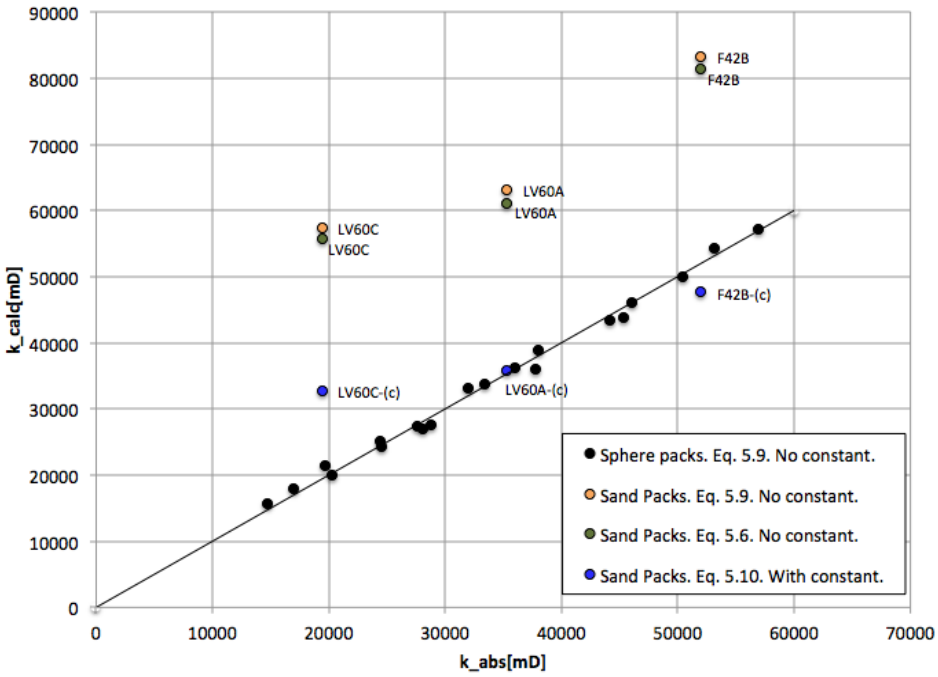

Figure 5.13: Precision of equation 5.6 and 5.9 on sand packs and equation 5.10 on sand packs. Equations are tested on sand packs from Imperial College London (2017); LV60C LV60A and F42B. Note the addition of the constant, c=0.57, and it's effect.

5.9 Formation Factor

As with the permeability, the formation factor of each of the sphere packs was found from e-Core. The simulated formation factors are presented in table 5.2. e-Core calculates the formation factor solving the Laplace equation with conservation of electrical charge. From

the table we note that for each increase in standard deviation the formation factor increases along. This applies to each of the mean grain sizes. The increase is due to the enhanced complexity of the pore structure when the standard deviation increases. This gives a rise in the resistivity of the rock filled with water and thus a higher formation factor.

Another aspect worth noting from the simulated formation factors is the little to no fluctuation of the values. The difference between the largest and smallest value is 0.86. Berg (2017) arrived at the following equality in his paper:

$$F = \frac{C}{\tau^2 \phi}, \tag{5.11}$$

where C is the constriction factor, τ is the tortuosity and ϕ is the porosity. Since the porosity and formation factors of the sphere packs are known, we are able to express $\frac{C}{\tau^2}$. This relation characterizes the pore structure and says something about the structural variation of the porous medium. From all the sphere packs we end up with values that are close to consistent and showing stable behavior. This indicates that the structural variation of the model is modest. This was expected as one understand that the possible variation in the pore structures of sphere packs is limited.

MGS	SD	F	ϕ	$\frac{C}{\tau^2}$
175	15	4.11	39.5	162.1
175	30	4.27	38.5	164.4
175	45	4.54	36.8	167.0
175	60	4.81	35.2	169.3
175	75	5.03	34.0	171.0
200	15	4.05	39.6	160.3
200	30	4.16	38.8	161.4
200	45	4.34	37.7	163.5
200	60	4.56	36.2	165.0
200	75	4.83	34.7	167.2
225	15	4.00	39.7	158.6
225	30	4.06	39.1	159.0
225	45	4.22	38.2	161.1
225	60	4.46	36.6	163.1
225	75	4.66	35.3	164.6
250	15	3.97	39.8	157.7
250	30	4.07	39.0	158.9
250	45	4.12	38.5	158.8
250	60	4.26	37.6	160.1
250	75	4.49	36.2	162.5

Table 5.2: Simulated formation factors of the sand packs performed in e-Core. The ratio between the constrictions and tortuosity has little variation, indicating little structural variation.

CHAPTER 6

DISCUSSION

In the following chapter the results obtained and procedures performed to achieve the results will be discussed. The two approaches are assessed and parameters used in both methods will be evaluated. Further, rock transport and geological properties will be discussed. Lastly, the applicability and the equations restrictions will be deliberated.

6.1 Comparison with Other Empirical Equations

The Darcy equation has served as a basis for nearly all equations calculating flow in porous media. The equations developed from it are usually altered and the findings have been based on data provided by experiments. Empirical factors have been added to the equations to better fit observed data. Other scientists have expressed transport properties relating it to size parameters. In table 6.1 below, some of the existing empirical equations are used to compare it's accuracy versus equation 5.6 and 5.10.

From the table we can see that equation 5.10 performs very well compared to the other equations. It has the highest degree of precision. For sand pack LV60C Krumbein and Monk's (1943) equation outperforms all the others.

Case	k.abs	Eq. 5.6	Eq. 5.10	Krumbein	Berg	Hazen	Katz-T
F42B	52000	81429	47638	31336	59205	60778	51725
LV60A	35300	61115	35798	23591	83809	45009	61533
LV60C	19400	55735	32751	21647	73193	40825	46939

Table 6.1: Comparison with some of the empirical equations existing. All permeabilities are expressed in millidarcies.

6.2 Implications of the Results and Findings

The results obtained from the simulations and calculations performed yielded two equations that deliver permeabilities within a reasonable accuracy. By studying the relationships developed and the details of the methodology used to obtain these relationships, there are a few elements that may cause inaccuracies. These may be inaccuracies involving constants, use of different statistical measures, and basic workflow. When evaluating the equations, one of the elements that appear to affect the relationship between a grain size distribution and permeability is the standard deviation.

For the sand packs from Imperial College London (2017) the cumulative raw grain size distribution was extracted and compared to the cumulative distribution generated from it's volume-weighted mean and standard deviation. In appendix C this is showcased for each sand pack. It became evident that the raw distribution and the distribution volume weighted based on mean and standard deviation, did not match each other to a degree of acceptable precision. By increasing the standard deviation we visually got a better match between the curves as shown in figure 6.1.

This suggests that a higher standard deviation will give a better match. The standard deviation utilizes the mean grain size as an input. Mean is known to be sensitive when applied to a distribution that has "outliers" or extreme values, either small or large (Campbell and Swinscow, 2009). It is also sensitive to skewed distributions, which might be the case for a grain size distribution (Blott and Pye, 2001). The possibility of extreme values or skewed distribution might be the explanation to the discrepancy in standard deviation when mean value is applied. A better value for such distributions could have been the median. The median handles extreme values and better describe the central tendency (Manikandan, 2011). This belief was confirmed when the mean and the median of the sand packs was compared. By changing the mean with the median, there is a slight increase in the standard deviation. Although there is an apparent effect, this is of a rather small impact.

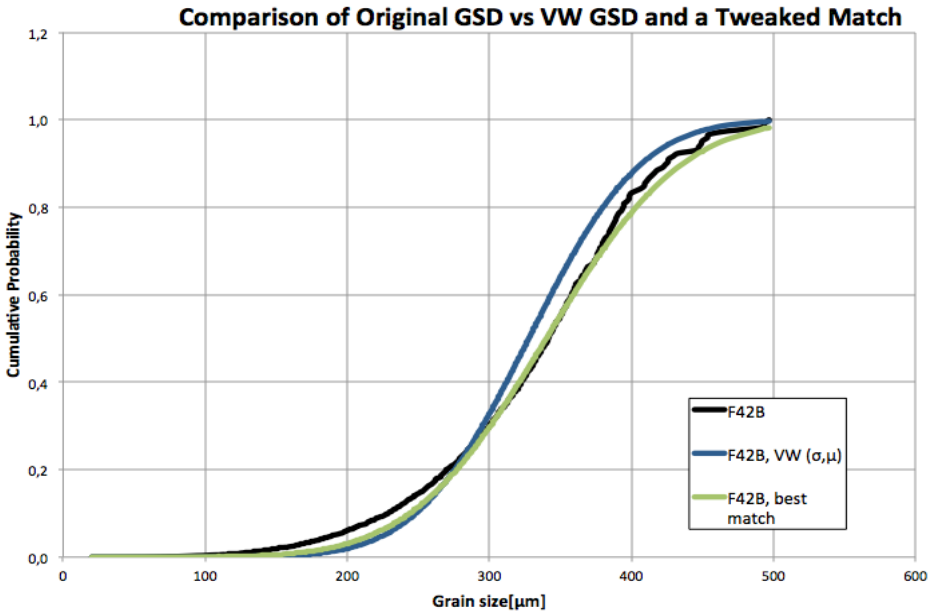

Figure 6.1: The actual grain size distribution is seen as the black curve, while the volume weighted distribution based on mean and standard deviation is blue. By increasing the standard deviation, σ, we are able to get a closer match (green).

6.3 Pore Scale Defects

As presented in section 5.7, a pre-factor was added to the equation to reduce the error of permeability when applied to sand packs. A further investigation was done on a pore scale level to study the texture properties and their effect on pore throats. First, the sand packs in regard were simulated through sedimentation in e-Core. From this simulation a 2D model of the rock was examined to find a pore throat for inspection. This was done moving up and down through the rock in the x-direction. When a pore throat was located, it was made sure that this was at the point where the grains had their largest cross section, i.e. the largest diameter. The section of interest was imaged using the snipping tool. Inkscape was used for outlining the grains and pore area, and color them with an individual color, as seen in figure 6.2. Secondly, the picture was imported into ImageJ, where the picture was transformed into a 8-bit monochrome and it's pixel count extracted. From the pixel count extracted one is able to calculate the ratio of grains to pore area and compare this to the pore area estimated from the MATLAB code (A.2) for the same grains.

Preliminary tests of equation 5.9 showed that it was overestimating permeability when applied to real sand packs, as seen in section 5.7. The samples in regard have different

sorting and packing than the sphere packs, and the grains have different size, shape and orientation. The overestimation was interpreted to be an effect of a combination of these factors. By conducting a simple test, as described above, on a pore throat from the sand pack-LV60C, we found the ratio between the real pore throat area and the calculated. From this we are able to propose a constant accounting for the difference.

From the analysis it became clear that the green pore space in figure 6.2 was estimated to have a higher area than the one calculated when using the MATLAB code presented in appendix A.2. This implies that there are properties of the pore space in the sand packs that affect the size of the pore area making it bigger than the one estimated from MATLAB. One of the aspects that is believed to be of considerable impact is the massive grain contacts seen in the thin section (fig. 6.2). They are not remotely close to the one-point grain contacts in the sphere packs. The texture effects of the grains, angularity and orientation, will also influence the formation of pores as these properties will not let the grains create the small pores we see in the sphere packs. Based on the simple test described, the ratio between the pore throats was found to be 0.85. This supports the pre-factor that was added in section 5.7 and substantiates the believed effect of the grain contacts and texture properties.

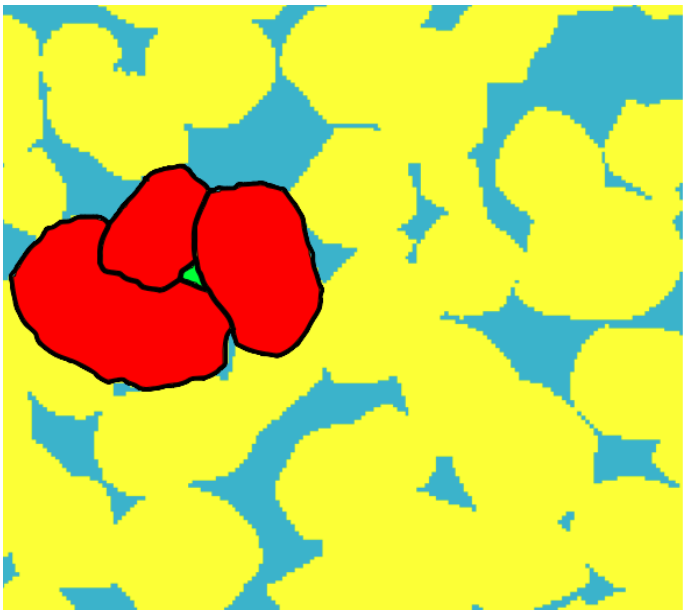

Figure 6.2: Thin section of three grains in a sand pack. Blue is pore space, yellow is grains, the three red grains are the ones analyzed along with the green pore area. Picture is taken from the 2D representation given by e-Core when sand packs are simulated.

The factor of 0.85 is based on a raw and simplistic analysis and interpretation. The main issue of this factor is that analysis was only performed on a single pore throat in a single sand pack. By conducting an analysis on a larger number of sand packs and with numerous of pores in each sand pack the factor would have been more representative. Outlining of the three grains was done thoroughly, but it is likely that some of the grain area have been excluded using the marker. These minor discrepancies may lead to some error in the proposed constant. Another aspect is the grain contacts, which were done solely by interpretation. The contacts might be incorrect or grains might overlap and the interpretation was done in two dimensions only. Thus, there are many uncertainties and inaccuracies regarding the calculation of this factor.

Fatt (1956) stated in his paper that the ones that had previous developed equations describing flow in porous media had found *"agreement between theory and observation (...) by inserting parameters of doubtful physical significance"*. Although, the constant proposed in this thesis is based on the fact that the massive grain contacts, angularity and orientation do affect the pore throat, it may be seen as a parameter of doubtful physical significance. This is understandable, as we used it as a fitting factor. Fraser (1935) states that well-rounded grains pack with a minimal pore space, but when angularity increases the porosity and permeability should expect an increase as well. Further, Beard and Weyl (1973) propose that this increase can be due to bridging of pores because of higher angularity and looser packing. Both papers support the idea of a factor as they say that the pore throat of sphere packs will have a smaller area than of sands with angular grains, as is the understanding stated in section 5.7. This supports the proposed factor and defends it's physical significance.

From section 5.9 and table 5.2 we saw that the structural variation of the created sphere packs was moderate. This was suspected, as there can be little variation in such simple porous media. The fifth column in table 5.2, representing $\frac{C}{\tau^2}$, shows stable behavior, and indicates that the tortuosity and constrictions for the different sphere packs is relatively constant. From Berg and Held (2016), we can use the following equation:

$$k = \frac{\tau_s^2 l_h^2 \phi_s}{8 C_s}, \tag{6.1}$$

where τ_s is the average tortuosity of streamline lengths, l_h is the hydraulic characteristic length, ϕ_s is the pore space that is accessible for fluid flow and C_s is the constriction factor defining the variation in pore sizes along the flow paths. Thus, the only property that differs between the sphere packs controlling the ability for flow is the pore throat diameter, here expressed as l_h.

6.4 Testing Equation on Discontinuous GSD

Equation 5.9 showed to cope well with the large grain size distributions, as the sand packs contained up to 14000 values. These and the sphere packs are all distributions with a cumulative grain size distribution that is smooth. This means that they do not have any large transition from one bin size to another. In other words the bin sizes show continuous behavior. What if a rough and stair-like volume weighted distribution was used as input?

A few distributions were made constituent of between 132 and 20 grains with a discontinuous cumulative grain size distribution. The cumulative grain size distributions can be seen in figure 6.3. These distributions were then tested using the code finding expected inscribed diameter as seen in appendix A.7 and permeabilities calculated using equation 5.9. The result of the test is shown in figure 6.4.

The permeabilities calculated from equation 5.9 for the broken distributions align pretty well with each other. They end up being a little underestimated compared to the sphere packs with a smooth distribution. Although, underestimating permeabilities, we can say that this supports the relation discovered as they all are affected similarly.

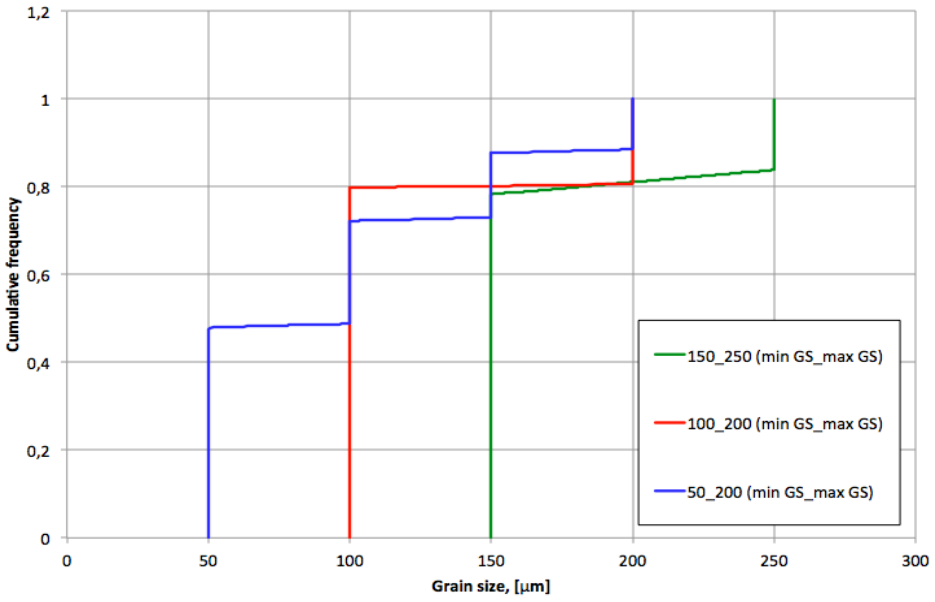

Figure 6.3: Discontinuous cumulative grain size distributions.

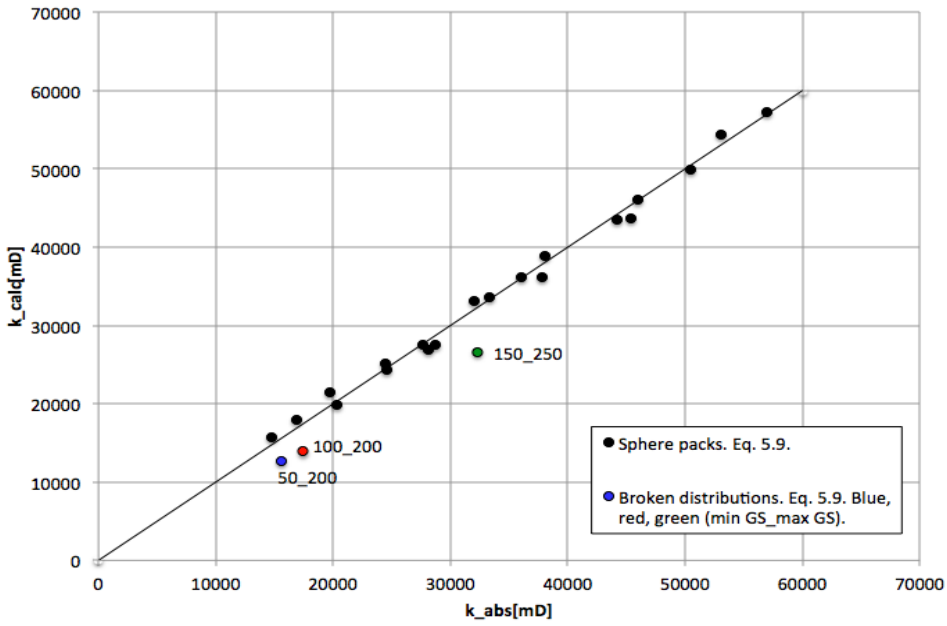

Figure 6.4: Permeability of discontinuous grain size distributions as presented in figure 6.3 calculated using equation 5.9.

6.5 Volume Weighting

As described earlier a volume weighting of the grain size distributions was performed. This was done with a belief that it would create a more realistic distribution of the grains. Main contributor for this was that the smallest grains were underrepresented volume wise. By volume weighting the aim was to better represent natural porous media consisting of throats and pore space filled with smaller grains.

In figure 6.5, equation 5.9 is tested on a non-volume weighted grain size distribution. As one can see from the figure we end up with four horizontal trends, one for each mean grain size. The movement leftwards from the linear trend is due to increasing standard deviation. Thus, we can say that increasing standard deviation increases the error of the calculated permeability versus the absolute. This is interpreted to be due to the increased amount of large grains compared to smaller volume wise, such a situation is described in section 2.10. With a high standard deviation larger grains dominate the pore structure giving favorable properties for fluid flow. The smallest standard deviation practically falls on top of the linear trend due to a more uniform grain size distribution. The believed hypothesis is further strengthened from this investigation.

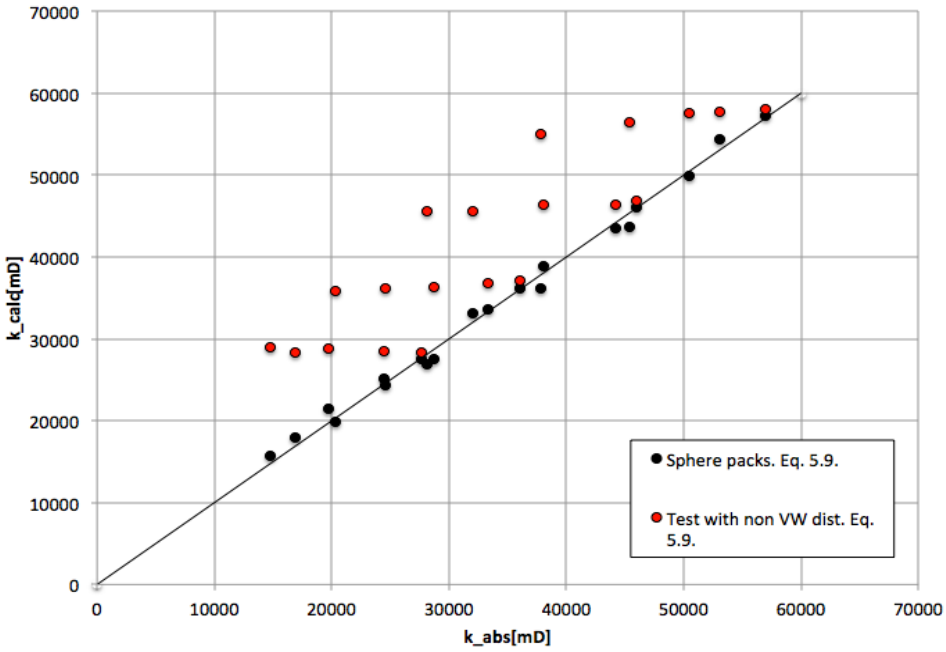

Figure 6.5: Test of equation when applied to a non volume weighted distribution. Note the horizontal trend of each grain size for the non VW distribution, for every increase in standard deviation the error becomes larger.

6.6 Applicability

Fatt (1956) stated in his paper that equations describing flow in porous media "*are only as valid as is the model used in their development*". The sphere pack model that forms the basis of this study also shapes the applicability of the proposed equation. Equation 5.9 gives permeability of high accuracy for the volume weighted sphere packs, but is not as precise for real sand packs. Thus, the equation is most precise when used on the model itself and this confirms Fatt's statement. Hence, the proposed factor as described in section 5.7. One can say that creating a general model constricts the final equation to the model that the equation was developed from.

Another parameter that constrains the equation is that all of the simulated packs is within five porosity percent, between 34-39%. Such a small variation in the porosity may lead to an equation that is not applicable to reservoirs constituent of rocks with a porosity higher or lower than these. An additional element to consider is that a larger span of porosities could have revealed possible non-linearity effects.

6.7 Sphere Packs as Analogs for Rock Samples

The sphere packs that the equations are based on are well sorted and constituent of ideal spheres. In reality there are no rocks like that, and the sphere pack model thus creates a very simplistic rock. A relative realistic rock would have included clays and angular grains of various sorting. Compaction is excluded in the creation of the sphere packs leading to loose packing. Another aspect of excluding compaction is that the grains will not experience compression and pressure solution. The net result of excluding these effects is that porosity and permeability is higher than for typical oil reservoirs.

After sedimentation and compaction, burial of the geological area begins and temperature and pressure increases and one reach the region where diagenesis occurs. Diagenesis is a process altering the rock and where growth of new minerals (authigenesis), such as clay and cements occur. Cementation of the pore space drastically reduces porosity and kills pore throats, leading to no fluid flow. Clay is known to reduce the permeability, as it's minerals may break loose from it's host grains when there are high flow rates. The broken minerals migrate with the flow, blocking pore throats. Understandably, the effects of diagenesis are multiple and it has a great impact on a rocks ability to contain and transmit fluids.

If the two factors above had been accounted for and implemented into the equation, it is expected that the permeabilities would have been lower and the equation more precise when applied to sand packs. The problem with these factors is that they are hard to quantify. If quantified and implemented the applicability of the equation had been wider.

CHAPTER 7

CONCLUSION

The objective of this thesis was to study the transport properties of porous media and investigate the relation between a grain size distribution and permeability. Further, the ambition was to express permeability as a function of grain size distribution properties and characteristics of the pore area. The base of the experimental investigation was that permeability was expected to be correlated to mean grain size, standard deviation and characteristics of the pore area. The main findings of this investigation are:

- The results show that there is a relationship between transport properties of porous media and both a grain size distribution and the expected inscribed diameter of the pore area.
- Expressing permeability as a function of mean grain size and standard deviation proved to better estimate permeability than using pore area characteristics. Both equations yields results within a reasonable accuracy for clean sandstones of good sorting.
- Manual optimization of the equation expressing permeability through pore area characteristics suggest a factor $c \simeq 0.57$ should be included. Image analysis of pore throats supports this. With the factor included the equation yields permeabilities with a high degree of precision for sand packs.
- Equation 5.9 does not break down when applied to discontinuous grain size distributions.

- The equations developed has a narrow field of applicability.
- The outcome of this investigation supports the believed correlation between mean grain size, standard deviation and characteristics of the pore area and permeability.

CHAPTER 8
FURTHER WORK

The relationships developed in this thesis showed to give satisfactory results for simple sphere packs, but did not perform to a satisfactory degree when applied to natural porous media. With an included factor, the equation performed well. Further research and development is needed, and for further work the following should be considered:

- Further investigate texture properties that may impact the pore throats. This includes, sphericity, grain contacts and overlapping. These properties and their effect should also be quantified and included in the equation.
- Look into use of other models for quantifying flow in porous media, for example, a network model.
- Investigate the possibilities of including compaction in the model that serves as basis for developing the equations. This would make the equations more realistic, but may restrict the equations applicability.
- Thoroughly study the effects of volume weighting the grain size distribution and look at other possible approaches.
- A further development of the method expressing permeability using expected inscribed diameter of the pore area. Possibly look at other geometrical properties of the pore area.
- Utilize optimization techniques for minimizing the possible errors when generating the equation.

- Conduct tests on a larger amount of thin sections acquired from both digital rock physics and real rocks for different rock samples. A larger amount of sand packs would make the proposed pre-factor more representative.

BIBLIOGRAPHY

American Petroleum Institute, 1998. Recommended Practices for Core Analysis. API Publishing Services.

Andrä, H., Combaret, N., Dvorkin, J., Glatt, E., Han, J., Kabel, M., Keehm, Y., Krzikalla, F., Lee, M., Madonna, C., Marsh, M., Mukerji, T., Saenger, E. H., Sain, R., Saxena, N., Ricker, S., Wiegmann, A., Zhan, X., 2013. Digital Rock Physics Benchmarks—Part I: Imaging and Segmentation. Computers & Geosciences 50, 25–32.

Archie, G., 1942. The Electrical Resistivity Log as an Aid in Determining Some Reservoir Characteristics. Transactions of the AIME 146 (01), 54–62.

Beal, C., 1946. The Viscosity of Air, Water, Natural Gas, Crude Oil and Its Associated Gases at Oil Field Temperatures and Pressures. Transactions of the AIME 165 (01), 94–115.

Beard, D. C., Weyl, P. K., 1973. Influence of Texture on Porosity and Permeability of Unconsolidated Sand. The American Association of Petroleum Geologists Bulletin, 57 (2), 349–369.

Bellini, S., Azzato, G., Grandinetti, M., Stellato, V., Marco, G. D., Sun, Y., Caravella, A., 2018. A Novel Connectivity Factor for Morphological Characterization of Membranes and Porous Media: A Simulation Study on Structures of Mono-Sized Spherical Particles. Applied Sciences 8 (4), 573.

Berg, C. F., 2012. Re-examining Archie's law: Conductance description by tortuosity and constriction. Physical Review E 86 (4).

Berg, C. F., 2014. Permeability Description by Characteristic Length, Tortuosity, Constriction and Porosity. Transport in Porous Media, 103 (3), 381–400.

Berg, C. F., 2017. Fontainbleau 3D models - Grid model 21. https://www.digitalrocksportal.org/projects/57/origin_data/285/, accessed: 01.09.2017.

Berg, C. F., Held, R., 2016. Fundamental Transport Property Relations in Porous Media Incorporating Detailed Pore Structure Description. Transport in Porous Media 112 (2), 467–487.

Berg, C. F., Lopez, O., Berland, H., 2017. Industrial Applications of Digital Rock Technology. Journal of Petroleum Science and Engineering 157, 131–147.

Berg, R. R., 1970. Method for Determining Permeability from Reservoir Rock Properties. Gulf Coast Association of Geological Societies Transactions 20, 303–317.

Blott, S. J., Pye, K., 2001. GRADISTAT: a grain size distribution and statistics package for the analysis of unconsolidated sediments. Earth Surface Processes and Landforms 26 (11), 1237–1248.

Campbell, M. J., Swinscow, T. D. V., 2009. Statistics at Square One. BMJ Books.

Carman, P. C., 1937. Fluid Flow Through Granular Beds. Chemical Engineering Research & Design 75, S32–S48.

Carrier, W. D., 2003. Goodbye, Hazen; Hello, Kozeny-Carman. Journal of Geotechnical and Geoenvironmental Engineering 129 (11), 1054–1056.

Darcy, H., 1856. Les fontaines de la ville de Dijon. Dalmont, Paris. Atlas, 590–594.

Diamond, S., 2000. Mercury porosimetry: An inappropriate method for the measurement of pore size distributions in cement-based materials. Cement and Concrete Research 30 (10), 1517–1525.

Engeskaug, K., 2017. A Numerical Investigation of the Relation Between Grain Size Distribution and Permeability. TPG4560 - Petroleum Engineering, Specialization Project.

Fatt, I., 1956. The network model of porous media, I. Capillary pressure characteristics. Physical Review E 207, 144–159.

Fraser, H. J., 1935. Experimental Study of the Porosity and Permeability of Clastic Sediments. The Journal of Geology 43, 910–1010.

Graton, L. C., Fraser, H. J., 1935. Systematic Packing of Spheres - With Particular Relation to Porosity and Permeability. The Journal of Geology 43 (8, Part 1), 785–909.

Hazen, A., 1895. The Filtration of Public Water-Supplies. Wiley.

Hu, X., Hu, S., Jin, F., Huang, S., 2017. Physics of Petroleum Reservoirs. Petroleum Industry Press and Springer-Verlag Berlin Heidelberg.

Hunt, A., 2014. Percolation Theory for Flow in Porous Media. Springer.

Imperial College London, 2017. Micro-CT Images and Networks. http://www.imperial.ac.uk/earth-science/research/research-groups/perm/research/pore-scale-modelling/micro-ct-images-and-networks/, accessed: 20.11.2017.

Jualbatusplit, 2014. Ukuran standar coarse aggregat bag.3. saringan. https://jualbatusplit.wordpress.com/2014/08/20/ukuran-standar-coarse-aggregat-bag-3-saringan/, accessed: 12.12.2017.

Katz, A. J., Thompson, A. H., 1986. Quantitative prediction of permeability and electrical conductivity in porous rock. In: SEG Technical Program Expanded Abstracts 1986. Society of Exploration Geophysicists.

King, H., 2017. Sedimentary rocks. http://geology.com/rocks/sedimentary-rocks.shtml, accessed: 10.10.2017.

Kozeny, J., 1927. Ueber Kapillare Leitung des Wassers im Boden. Sitzungsber Akad. Wiss. 136 (2a), 271–306.

Krumbein, W. C., 1936. Application of Logarithmic Moments to Size Frequency Distributions of Sediments. SEPM Journal of Sedimentary Research Vol. 6.

Krumbein, W. C., Monk, G. D., 1943. Permeability as a Function of the Size Parameters of Unconsolidated Sand. Society of Petroleum Engineers 151 (Issue 1), 153–163.

Lagarias, J. C., Mallows, C. L., Wilks, A. R., 2002. Beyond the descartes circle theorem. The American Mathematical Monthly, 109 (4), 338–361.

Manikandan, S., 2011. Measures of central tendency: Median and mode. Journal of Pharmacology and Pharmacotherapeutics 2 (3), 214–215.

Mason, G., Morrow, N. R., 1991. Capillary Behavior of a Perfectly Wetting Liquid in Irregular Triangular Tubes. Journal of Colloid and Interface Science, 141 (1), 262–274.

Mualem, Y., 1976. A New Model for Predicting the Hydraulic Conductivity of Unsaturated Porous Media. Water Resources Research, 12 (3), 513–522.

Numerical Rocks AS, 2012. e-Core User Manual. Numerical Rocks AS.

Øren, P.-E., Bakke, S., Arntzen, O. J., 1998. Extending Predictive Capabilities to Network Models. SPE Journal, 4 (3), 324–336.

PoreLab, 2018. Research. `https://porelab.no/research/`, accessed: 20.04.2018.

Retsch GmbH & Co. KG , 2004. The Basic Principles of Sieve Analysis. Retsch GmbH & Co. KG.

Scheidegger, A. E., 1957. The physics of flow through porous media. University of Toronto Press.

Slichter, C. S., 1899. Theoretical Investigation of the Motion of Ground Waters. U.S. Department of the Interior, Geological Survey, Water Resources Division, Ground Water Branch.

Soddy, F., 1936. The Kiss Precise. Nature 137 (3477), 1021–1021.

Sutera, S. P., Skalak, R., 1993. The History of Poiseuille's Law. Annual Review of Fluid Mechanics, 25 (1), 1–19.

Xiong, Q., Baychev, T. G., Jivkov, A. P., 2016. Review of pore network modelling of porous media: Experimental characterisations, network constructions and applications to reactive transport. Journal of Contaminant Hydrology, 192, 101–117.

APPENDIX A
PROGRAMMING

A.1 Script Generating Readable File for e-Core, binGenerator2.py

```
1  #import numpy as np
2  import math as m
3  import sys
4
5  inputfile=sys.argv[1]
6  input=open(inputfile,'rU')
7  lines=input.readlines()
8  outputfile=sys.argv[2]
9  ofile=open(outputfile,'w')
10
11 for ii in range(0,len(lines)):
12     line=lines[ii]
13     for jj in range(0,int(line.split()[1])):
14         #print input[ii][0]
15         ofile.write(line.split()[0]+'\n')
16
17 ofile.close()
```

A.2 Calculating Pore Area

```
function porearea = area2(r1,r2,r3)
%a=((r1+r2)^2+(r1+r3)^2-(r3+r2)^2)/(2*(r1+r2)*(r1+r3))
%acos(a)
%Expressing the angles of the triangle
alpha=acos(((r1+r2)^2+(r1+r3)^2-(r3+r2)^2)/(2*(r1+r2)*(r1+
    r3)));
beta=acos(((r1+r2)^2+(r3+r2)^2-(r1+r3)^2)/(2*(r1+r2)*(r3+r2
    )));
gamma=acos(((r1+r3)^2+(r3+r2)^2-(r1+r2)^2)/(2*(r1+r3)*(r3+
    r2)));
%Calculating the height of the triangle
A=0.5*(r3+r2)*(r1+r3)*sin(gamma);
%B, C and D are the circle sectors of each grain
B=(r1^2/2)*alpha;

C=(r2^2/2)*beta;

D=(r3^2/2)*gamma;
%Full pore throat area
porearea=A-B-C-D

%Calculating circumference, s
b1=r1*alpha;
b2=r2*beta;
b3=r3*gamma;
circ=b1+b2+b3

%Calculating Shape factor
G_shape=porearea/((circ)^2)

%Calculating inscribed radius
k1=1/r1;
k2=1/r2;
k3=1/r3;
rinsc=1/(k1+k2+k3+2*sqrt(k1*k2+k2*k3+k3*k1))
%Inscribed area:
```

```
34 Area_inscribed=pi()*rinsc^2
35
36
37 end
```

A.3 Random Area Matrix Generator

```
1  function area=randArea(datavek,n)
2  %creating a matrix of zeroes with dimensions n^2*n
3  area=zeros(n^2,n);
4  %Double for-loop, calculating the different areas from
       area2, by picking
5  %random values from datavek
6  for i=1:n^2
7      for j=1:n
8          area(i,j)=area2(datavek(randi([1 length(datavek)]))
               ,datavek(randi([1 length(datavek)])), datavek(
               randi([1 length(datavek)])));
9      end
10 end
11 end
```

A.4 Conductivity for Pore Area

```
1  meand=2*mean(datavek);
2  n=round(2500E-6/meand);
3  H=(randArea(datavek,n)).^2./(8.*pi().*meand);%calculating
       the Conductivity using Hagen-Poiseuille
4  C=sum(harmmean(H,2).*n)/(n*meand);%Harmonic mean of each
       row, then summing the conductivities from each
```

A.5 Conductivity for Pore Area with Shape Factor

```
meand=2*mean(datavek);
n=round(2500E-6/meand);

[A,G]=randAreashape(datavek,n);
H=(A).^2.*G.*3 ./(5.*meand);%calculating the Conductivity
    using Hagen-Poiseuille
C=sum(harmmean(H,2).*n)/(n*meand);%Harmonic mean of each
    row, then summing the conductivities from each
```

A.6 Inscribed Diameter

A.6.1 Calculating Inscribed Diameter

```
function dinsc=insc(r1,r2,r3)

%Using Descartes Theorem
k1=1/r1;
k2=1/r2;
k3=1/r3;

dinsc=2/(k1+k2+k3+2*sqrt(k1*k2+k2*k3+k3*k1));


end
```

A.6.2 Randomizer

```
function area=randinsc(datavek,n)

%creating a matrix of zeroes with dimensions n^2*n
area=zeros(n^2,n);
%Double for-loop, calculating the different areas from
    area2, by picking
%random values from datavek
```

```
for i=1:n^2
    for j=1:n
        area(i,j)=insc(datavek(randi([1 length(datavek)])),
            datavek(randi([1 length(datavek)])), datavek(
            randi([1 length(datavek)])));
    end
end
end
```

A.6.3 Variance and Mean Inscribed Diameter

```

meand=2*mean(datavek);%mean diameter of gsd
n=round(2500E-6/meand);%number of channels
checkvar=randinsc(datavek,n);%Creating matrix of random
    insc. diameters
[nx,ny]=size(checkvar);%resizing for calculating purposes
vekcheck=reshape(checkvar,[nx*ny,1]);%Reshaping
variansen=var(vekcheck);%calculating variance of the
    inscribed diameters
gjennomsnitt=10^6*mean(vekcheck);%mean
minsc=harmmean(randinsc(datavek,n));%harm. mean of each row
     of inscribed...
%diameters
minscfinal=max(minsc);%inscribed diameter
```

A.7 Expected Value of Inscribed Diameter

```

nydatavek=10^-6.*datavek.^-1;%Inverting the datavek
sumvec=sum(nydatavek);%sum of matrix
antall=numel(nydatavek);%number of values in matrix

xinv=(1/(antall))*sumvec;%Expected value of 1/X
inscdia=2/((3+2*sqrt(3))*xinv);%Expected inscribed diameter
```

APPENDIX B

TABLES

Table B.1: Simulation set up

Case	Mean GS(μ)	SD(σ)	Min. GS(μm)	Max. GS(μm)
1	150	15	120	180
2	175	15	145	205
3	200	15	170	230
4	225	15	195	255
5	250	15	220	280
6	150	30	90	210
7	175	30	115	235
8	200	30	140	260
9	225	30	165	285
10	250	30	190	310
11	150	45	60	240
12	175	45	85	265
13	200	45	110	290
14	225	45	135	315
15	250	45	160	340
16	150	60	30	270
17	175	60	55	295
18	200	60	80	320
19	225	60	105	345

20	250	60	130	370
21	150	75	0	300
22	175	75	25	325
23	200	75	50	350
24	225	75	75	375
25	250	75	100	400

APPENDIX C

SAND PACKS - COMPARISON OF VW CUMULATIVE DISTRIBUTION AND RAW CUMULATIVE DISTRIBUTION

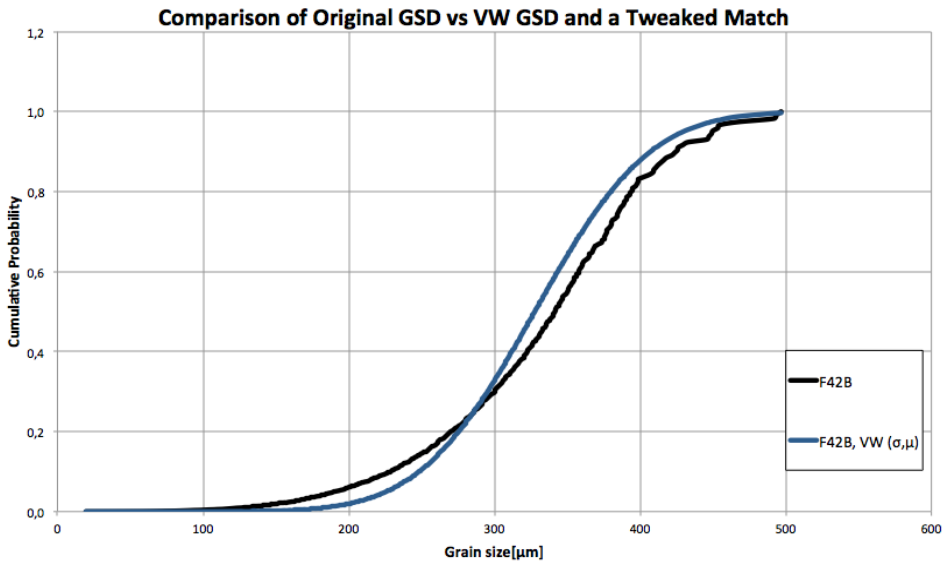

Figure C.1: F42B

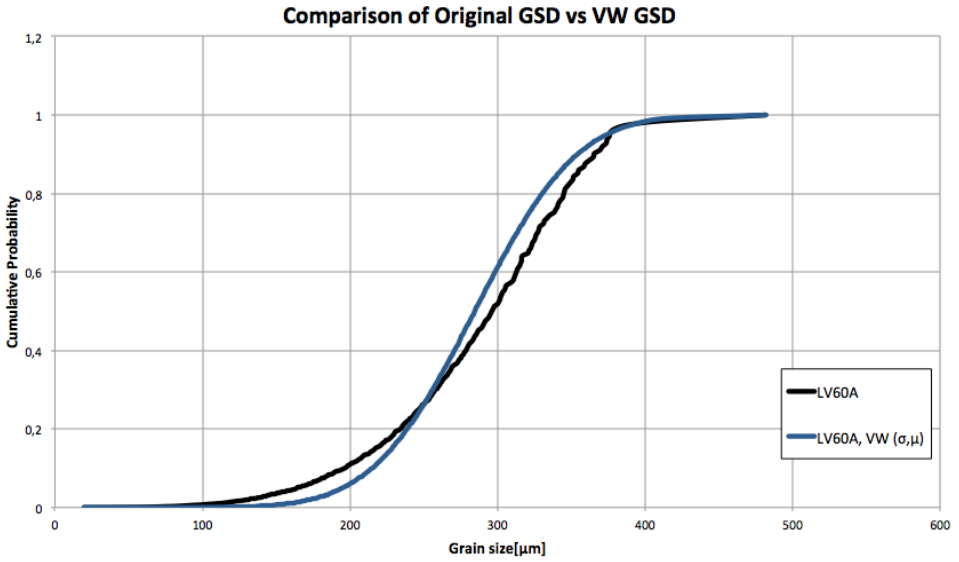

Figure C.2: LV60A

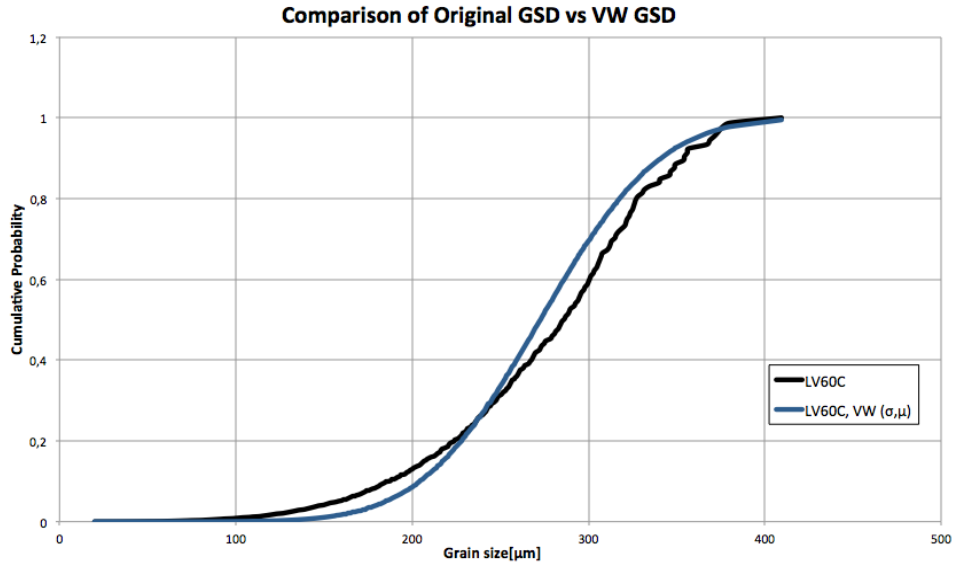

Figure C.3: LV60C

APPENDIX D

THE KISS PRECISE

For pairs of lips to kiss maybe
Involves no trigonometry.
This not so when four circles kiss
Each one the other three.
To bring this off the four must be
As three in one or one in three.
If one in three, beyond a doubt
Each gets three kisses from without.
If three in one, then is that one
Thrice kissed internally.

Four circles to the kissing come.
The smaller are the benter.
The bend is just the inverse of
The distance form the center.
Though their intrigue left Euclid dumb
There's now no need for rule of thumb.
Since zero bend's a dead straight line
And concave bends have minus sign,
The sum of the squares of all four bends
Is half the square of their sum.

To spy out spherical affairs

An oscular surveyor
Might find the task laborious, The sphere is much the gayer,
And now besides the pair of pairs
A fifth sphere in the kissing shares.
Yet, signs and zero as before,
For each to kiss the other four
The square of the sum of all five bends
Is thrice the sum of their squares.

in Nature, June 20, 1936 (Soddy, 1936).